AD-A131 247 LONGSHORE SAND TRANSPORT DISTRIBUTION ACROSS THE SURF ZONE DUE TO RANDOM WAVES(U) NAVAL POSTGRADUATE SCHOOL MONTEREY CA S M ABDELRAHMAN JUN 83 1/1

UNCLASSIFIED F/G 12/1 NL

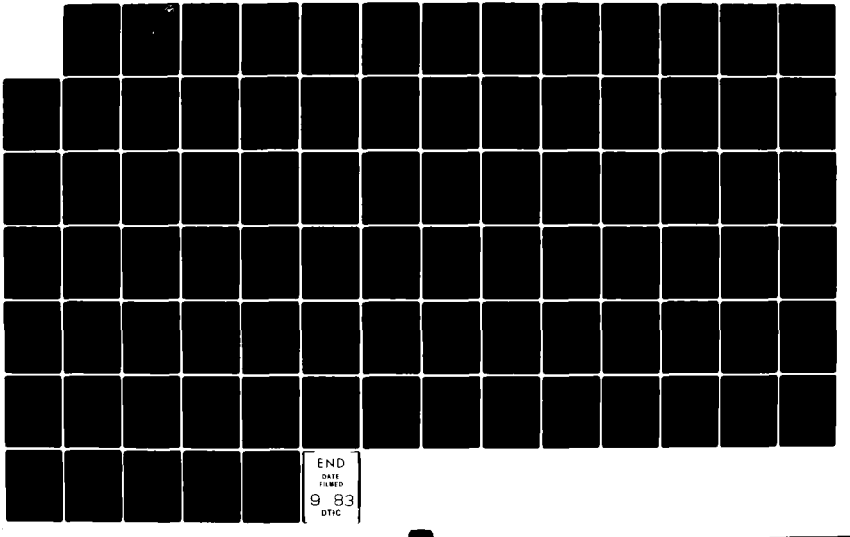

END
DATE FILMED
9 83
DTIC

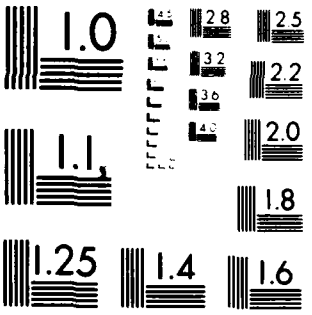

NAVAL POSTGRADUATE SCHOOL
Monterey, California

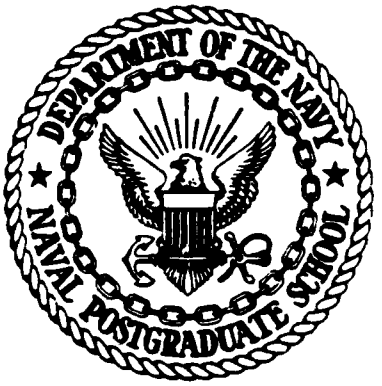

THESIS

LONGSHORE SAND TRANSPORT DISTRIBUTION
ACROSS THE SURF ZONE DUE TO RANDOM WAVES

by

Saad Mesbah M. Abdelrahman

June 1983

Thesis Advisor: E. B. Thornton

Approved for public release; distribution unlimited.

UNCLASSIFIED

SECURITY CLASSIFICATION OF THIS PAGE (When Data Entered)

REPORT DOCUMENTATION PAGE		READ INSTRUCTIONS BEFORE COMPLETING FORM
1. REPORT NUMBER	2. GOVT ACCESSION NO. AD-A131 247	3. RECIPIENT'S CATALOG NUMBER
4. TITLE (and Subtitle) Longshore Sand Transport Distribution Across the Surf Zone Due to Random Waves		5. TYPE OF REPORT & PERIOD COVERED Master's Thesis; June 1983
		6. PERFORMING ORG. REPORT NUMBER
7. AUTHOR(s) Saad Mesbah M. Abdelrahman		8. CONTRACT OR GRANT NUMBER(s)
9. PERFORMING ORGANIZATION NAME AND ADDRESS Naval Postgraduate School Monterey, California 93940		10. PROGRAM ELEMENT, PROJECT, TASK AREA & WORK UNIT NUMBERS
11. CONTROLLING OFFICE NAME AND ADDRESS Naval Postgraduate School Monterey, California 93940		12. REPORT DATE June 1983
		13. NUMBER OF PAGES 86
14. MONITORING AGENCY NAME & ADDRESS(if different from Controlling Office)		15. SECURITY CLASS. (of this report) Unclassified
		15a. DECLASSIFICATION/ DOWNGRADING SCHEDULE

16. DISTRIBUTION STATEMENT (of this Report)

Approved for public release; distribution unlimited.

17. DISTRIBUTION STATEMENT (of the abstract entered in Block 20, if different from Report)

18. SUPPLEMENTARY NOTES

19. KEY WORDS (Continue on reverse side if necessary and identify by block number)

sand transport numerical model

random waves

longshore current

20. ABSTRACT (Continue on reverse side if necessary and identify by block number)

Analytical and numerical models are developed to predict the longshore sand transport distribution across the surf zone. The models, which also predict the root mean square wave height, H_{rms}, and the longshore current, V, are compared with field data acquired from Leadbetter Beach, Santa Barbara, California, during the intensive storm period in February, 1980. The breaker coefficient, B, and the bed shear stress coefficient, c_f, when equal to 1.1 and 0.005, were found to give the best agreement between the predicted

DD FORM 1 JAN 73 1473 EDITION OF 1 NOV 65 IS OBSOLETE

S/N 0102-LF-014-6601

UNCLASSIFIED

SECURITY CLASSIFICATION OF THIS PAGE (When Data Entered)

#20 - ABSTRACT - (CONTINUED)

H_{rms} and V with the field measurements. The model for a plane sloping beach predicts the maximum sand transport at offshore distance X equal to $0.8X_b$, where X_b is the mean breakerline location, which agrees with Komar (1977a). The longshore sand transport formula, suggested by CERC (1977), is used to calibrate the model which requires the empirical transport coefficient B_s to be 0.18.

The sand transport cross-shore distribution predicted by the model does not agree well with the corresponding transport inferred from the field measurements. Reasons offered to explain the differences are (1) that the model does not include the swash zone where the maximum transport is found and (2) that beach profile information beyond a distance of 100 m offshore was incomplete. The results indicate the importance of including the swash zone to describe the effect of the long waves in predicting the sediment transport.

Approved for public release; distribution unlimited.

Longshore Sand Transport Distribution Across the Surf Zone Due to Random Waves

by

Saad Mesbah M. Abdelrahman
B.Sc. Civil Engineering, Alexandria University, Egypt, 1973

Submitted in partial fulfillment of the requirements for the degree of

MASTER OF SCIENCE IN OCEANOGRAPHY

from the

NAVAL POSTGRADUATE SCHOOL

June 1983

Author: _____

Approved by: Edward B. Thornton
Thesis Advisor

_____
Second Reader

_____
Chairman, Department of Oceanography

_____
Dean of Science and Engineering

ABSTRACT

Analytical and numerical models are developed to predict the longshore sand transport distributions across the surf zone. The models, which also predict the root mean square wave height, H_{rms}, and the longshore current, V, are compared with field data acquired from Leadbetter Beach, Santa Barbara, California, during the intensive storm period in February, 1980. The breaker coefficient, B, and the bed shear stress coefficient, c_f, when equal to 1.1 and 0.005, were found to give the best agreement between the predicted H_{rms} and V with the field measurements. The model for a plane sloping beach predicts the maximum sand transport at offshore distance X equal to $0.8X_b$, where X_b is the mean breakerline location, which agrees with Komar (1977a). The longshore sand transport formula, suggested by CERC (1977), is used to calibrate the model which requires the empirical transport coefficient B_s to be 0.18.

The sand transport cross-shore distribution predicted by the model does not agree well with the corresponding transport inferred from the field measurements. Reasons offered to explain the differences are (1) that the model does not include the swash zone where the maximum transport is found and (2) that beach profile information beyond a distance of 100 m offshore was incomplete. The results indicate the importance of including the swash zone to describe the effect of the long waves in predicting the sediment transport.

TABLE OF CONTENTS

LIST OF TABLES

LIST OF FIGURES

ACKNOWLEDGMENTS

First, I would like to express my appreciation to Prof. Edward B. Thornton for his encouragement, patience and assistance during this study. I would also like to thank Ms. Donna Burych for her assistance in providing data from field measurements.

I. INTRODUCTION

Water waves are one of the principal causes of shoreline changes. When waves break along the shore, they release their energy and momentum and give rise to a longshore current. The longshore current, along with the stirring action of the waves, is the primary mechanism for longshore sediment transport. The longshore sand transport rate is an essential factor determining erosion or accretion along a coast. If the longshore sand transport rate can be accurately estimated, a quantitative picture of shoreline evolution can be evaluated, including changes of the shoreline due to marine structures.

In the present study, analytical and numerical models are developed based on a longshore current model for random waves by Thornton and Guza (1983) and a sediment transport formulation by Thornton (1973) to predict the cross-shore sediment transport distribution and to compute the total volume of sand transport rate. The model is compared with the field data acquired from Leadbetter Beach, Santa Barbara, California (January-February, 1980).

The experiment at Santa Barbara was conducted as part of the Nearshore Sediment Transport Study (NSTS). The objectives of NSTS are to develop improved techniques and engineering formulae to predict sediment transport on beaches having straight and parallel contours by utilizing field measurements of waves and currents at several nearshore sites.

During the Santa Barbara experiment, beach profiles were measured daily along with extensive measurements of waves and currents. A severe storm attacked the site of the experiment during 16-20 Feb., 1980 causing significant changes in the shoreline configuration and beach profiles. Despite the destruction of most of the instruments during the storm, a very substantial and valuable record of waves and currents was acquired which makes the Santa Barbara data very unique and significant for nearshore sand transport studies.

The present work emphasizes the data acquired on 17 and 18 February, 1980. A strong longshore current was observed due to storm waves approaching the beach at moderately large angles (6° at the breaker line) causing significant erosion in the beach profile. The daily beach profiles during the experiment (January-February) show no well defined bars or troughs and essentially have a stable point 95 m offshore, which did not appear affected by erosion or accretion. Thus, it is hypothesized that the changes in the beach profile are due to sand transport in the longshore direction alone, and the on-offshore transport is negligible. Furthermore, the longshore sand transport distribution across the surf zone, predicted by the model, is assumed to have a distribution similar to the net longshore sand transport calculated from the profile changes.

II. LONGSHORE SEDIMENT TRANSPORT

A. GENERAL

When waves approach the shoreline at an oblique angle and break, they generate a longshore current parallel to the shoreline. This current in turn interacts with the waves to produce a longshore sand transport. The movement of sand particles is usually divided into two, not always distinct, modes of transport: bed load and suspended load transport. The bed load is the result of sand grains being rolled along the bottom by the shear of water moving above the sediment bed and is maintained by grain-to-grain contact. Bed load is usually considered to be confined to within 10 cm of the bottom. In the suspended load mode, the generally finer grains are transported by currents after they have been lifted from the bed by turbulent action of the wave-induced vertical motion. The total sand transport is the sum of the contribution by bed and suspended load transport. The rate at which the total volume of sand is transported parallel to the shoreline is termed "longshore sand transport: Q_l". The two most successful and widely used approaches for estimating the longshore sand transport are an empirical wave power model and Bagnold's energetics model.

B. WAVE POWER MODEL

In the wave power model, the rate of total longshore transport Q_l is simply assumed proportional to the longshore

component of wave power (P_ℓ) at the breaker line to some power n (Watts, 1953a).

$$Q_\ell = K_1 P_\ell^n \tag{2.1}$$

where K_1 and n are coefficients to be determined empirically. Assuming straight and parallel depth contours, the onshore energy flux in the direction of wave propagation per unit length of the beach is $EC_g \cos\alpha$, where E is the energy density of the waves, C_g is the group velocity of the incoming waves, and α is the angle of the wave crests relative to the shoreline. Then, the longshore component of wave energy flux per unit length of the beach is given by:

$$P_\ell = (EC_g)_b \cos\alpha_b \sin\alpha_b \tag{2.2}$$

where the subscript b refers to the breaker line. Applying linear theory,

$$P_\ell = \tfrac{1}{8} \rho g H_b^2 C_g \cos\alpha_b \sin\alpha_b \tag{2.3}$$

where ρ is the water density, g is the gravitational constant and H is the wave height.

Watts (1953a) obtained the first field measurements by which the sand transport rate could be related to the local wave characteristics. Caldwell (1956) combined additional

data with those of Watts and found the coefficient (n) in (2.1) to be less than unity, and with a different proportionality coefficient (K_1) than Watts.

Inman and Bagnold (1963) interpreted field and laboratory data and obtained a linear relationship between Q_ℓ and P_ℓ, i.e., n equal to unity, which takes into consideration the immersed weight of beach material.

$$Q_\ell = \frac{K}{(1-a)(\rho_s-\rho)} P_\ell \qquad (2.4)$$

where ρ_s is the density of sand transport, a is the porosity of beach sediment (taken as 0.40) and K is a dimensionless proportionality coefficient.

Komar and Inman (1970) utilized sand tracers to measure longshore sand transport rates. Using this new data combined with data from Watts (1953a), Caldwell (1956) and others, they obtained 0.77 for the proportionality coefficient K by relating the immersed weight transport rate I_ℓ to P_ℓ

$$I_\ell = 0.77\ P_\ell \qquad (2.5)$$

For quartz-density sand, $\rho_s = 2.65 \times 10^3$ Kg/m^3, $K = 0.77$, equation (2.4) becomes,

$$Q_\ell = 6.8\ P_\ell \qquad (2.6)$$

where Q_ℓ in (2.6) is measured in units of m^3/day and P_ℓ in watts/meter. Komar and Inman use the root mean square wave height in (2.5) and (2.6) instead of the significant wave height, suggested by CERC (1977), to evaluate the P_ℓ term.

The relationships described in equations (2.5) and (2.6) are almost purely empirical with no real consideration of the sand transport mechanism. In addition, the coefficient 0.77 in equation (2.5) has a high degree of uncertainty

Longuet-Higgins (1972), in attempting to rationalize (2.2), points out that since the energy flux (EC_g) is a vector rather than a second order tensor, the longshore component of wave power (P_ℓ) can be written equivalently as the product of two physically meaningful quantities:

$$P_\ell = [E \frac{C_g}{C} \cos \alpha \sin \alpha]C = S_{xy} C \qquad (2.7)$$

where S_{xy} is the longshore component of the radiation stress and C is the phase speed of the waves. The radiation stress (S_{xy}) is shown by Longuet-Higgins (1972), among others, to be the principal driving force for longshore currents, and thus would be expected to be important in describing longshore sediment transport. Vitale (1981) compared the radiation stress (S_{xy}) and the wave power (P_ℓ) as predictors of the longshore sediment transport rate by conducting three-dimensional movable-bed laboratory tests and he found no major difference in choosing S_{xy} over P_ℓ to predict the longshore sediment transport.

C. BAGNOLD'S ENERGETICS MODEL

Bagnold (1963) relates the rate of immersed weight transport (I_ℓ) to the work done by waves and current. The mechanics of sand particle movement are described as a back-and-forth motion under the action of the wave orbital motion with essentially no net transport. Wave energy is expended in supporting and suspending the moving sand above the bed. Once the sediments are suspended, the presence of a unidirectional current superimposed on the to-and-fro motion can then produce a net drift of sediment. Bagnold (1963) derived the relationship:

$$i_\theta = K' \omega \frac{u_\theta}{u_o} \tag{2.8}$$

where i_θ is sediment transport per unit width in the direction θ determined by the unidirectional current u_θ, ω is the available wave power supporting the sediments above the bottom, u_o is the orbital velocity of wave motion, and K' is a dimensionless coefficient.

Inman and Bagnold (1963) specified the various parameters of waves at the breaker line and obtained:

$$I_\ell = K' (EC_g)_b \frac{v_b}{u_m} \cos \alpha_b \tag{2.9}$$

where u_m is the maximum horizontal orbital velocity of the waves. Equation (2.9) can be viewed as a general relationship

because it does not specify the cause of the longshore current v_b; it can be either tidal, currents of a cell circulation, wind generated, or due to oblique wave approach. Komar and Inman (1970) utilized their littoral drift measurements to test equation (2.9) and required K' to be equal to 0.28 to agree with their data. In terms of Q_ℓ and for quartz density sand, equation (2.9) is given by

$$Q_\ell = 2.5 \, (E C_g)_b \, \frac{v_b}{u_m} \qquad (2.10)$$

where Q_ℓ is in m^3/day and the wave and current parameters are in mKs units (watts/meter) (Komar, 1983). Wang and Chang (1979) found good agreement between their measurements along the bayshore of a barrier island in the Gulf of Mexico, and equation (2.9) for a coefficient K' = 0.18, where the longshore currents generally are due to local winds and tides.

Bowen (1981) applied Bagnold's equation to the problem of on-offshore sediment transport on beaches and then studied the special case of a normal incident wave and steady on-offshore currents (no longshore currents). The waves are described using Stokes second order wave theory and the mean on-offshore current using Longuet-Higgin's (1953) bottom streaming solutions. The model predicts an equilibrium beach profile as a function of the incident wave characteristics. Bowen's results support observations that steep beaches are generally coarse grained, and short period waves cause a beach to erode.

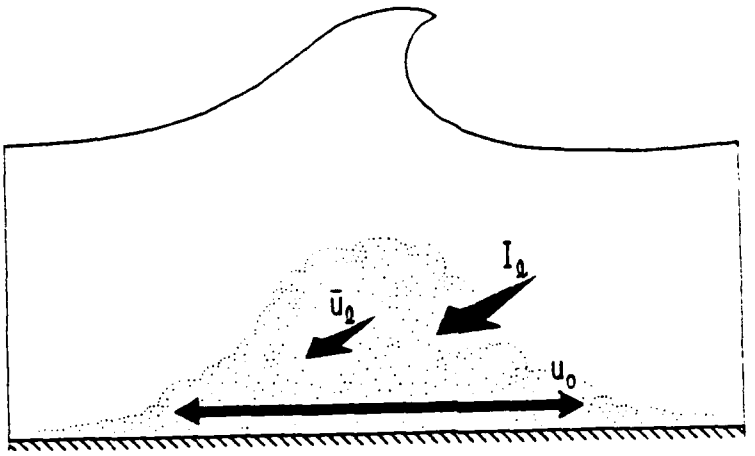

Figure (2.1). Schematic of the Bagnold model for sand transport wherein the orbital velocity u_0 due to the waves places the sand in motion, and the current $\bar{u}_\ell$ provides a net transport of sand, I_ℓ.

Bailard and Inman (1981) independently derived a very similar model to Bowen's (1981) to describe the instantaneous transport in the nearshore zone, including both on-offshore movements as well as longshore movement. An important part of the study is the effect of local bottom slope on sand transport rate, as this permits the analysis of the formation of the longshore bars and other inshore topography. Bailard (1982), extended the model to predict the total load transport for time-varying flow over an arbitrarily sloping planar bed. The model predicts the local equilibrium beach slope as well as the local near bottom sediment transport rate as a function of the near bottom velocity. Surf zone conditions are described as steady longshore and on-offshore currents in addition to a wave induced current having a local wave angle.

A number of other models have been proposed. For instance, Madsen and Grant (1976) adapt the Einstein-Brown sediment transport equations to time-varying sand movements under combined waves and unidirectional currents. The bottom stress (τ) under the combined oscillatory motions of the waves and any superimposed currents, and the resulting sand transport, vary with time. The model is relatively complicated and requires parameters for which no data are available. The success of the wave power formulation and Bagnold's energetics model is due to their relative simplicity requiring only one or two parameters specified from the data.

In general, the predictions of the littoral drift have a high degree of uncertainty. This partly results from our basic inability to make accurate measurements of sand transport on beaches. However, the two approaches of equations (2.5) and (2.9) can be used to give at least a qualitative description of littoral drift.

D. DISTRIBUTION OF LONGSHORE TRANSPORT ACROSS THE SURF ZONE

Bagnold's (1963) approach has been also utilized to predict the distribution of longshore sand transport. Thornton (1973) analyzed sand transport inside and outside the surf zone where the volume transport rate per unit width ($\bar{q}_s$) is given by:

$$\bar{q}_s = \frac{B_s}{g(1 - \frac{\rho}{\rho_s})} \left(\frac{v}{u_m}\right)^{1/2} \frac{\partial (EC_g)}{\partial x} \qquad (2.11)$$

where B_s is an empirical dimensionless coefficient. Thornton (1973) obtained field data at Fernandina Beach, Florida, to evaluate B_s in equation (2.11). The transport rate ($\bar{q}_s$) was measured using a series of bed load traps placed in a line across the nearshore. The results indicate that the maximum longshore transport is in the breaker zone with $B_s = 0.08$ and stronger transport occurs over the bars rather than in the troughs (Fig. 2.2).

Komar (1976b,1977a) similarly utilized Bagnold's (1963) model to analyze the distribution of the littoral drift in

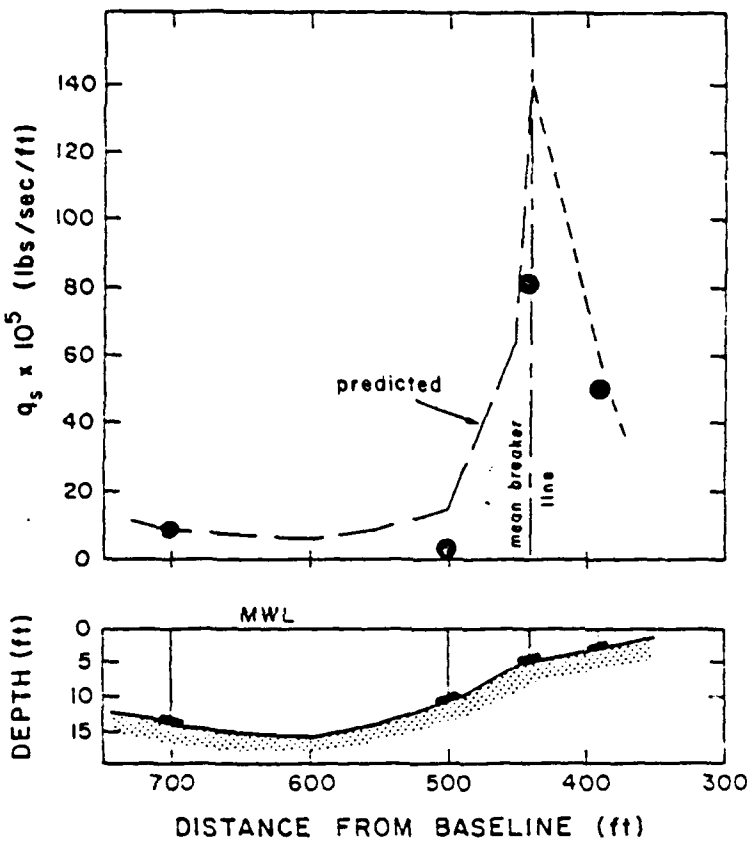

Figure (2.2). The distribution of the longshore sand transport measured by Thornton (1973) at Fernandina Beach, Florida, by bed load traps in the positions as shown. The dashed lines are based on equation 2.11 with $B_s = 0.08$. [from Thornton (1973)]

terms of (I_ℓ). The local immersed-weight of sand transport rate per unit of width inside the surf zone (i_x) is given by:

$$i(x) = \frac{\pi K_1}{4} (0.5\ C_f)\ \rho\ \gamma^2\ h(x)\ v(x) \qquad (2.12)$$

where C_f is the drag coefficient of oscillatory wave motions and h and v are the local water depth and longshore current, respectively; both are functions of the distance x offshore from the shoreline. K_1 is a dimensionless proportionality factor determined by calibrating the model equation (2.12) to yield I_ℓ calculated from equation (2.5) where the total immersed-weight transport can be evaluated by integrating $i(x)$ across the surf zone:

$$I_\ell = \int_0^{x_b} i(x)\ dx$$

where x_b is the surf zone width as shown in Fig. (2.3). Komar (1977a) calculated the distribution of both the longshore current and the longshore sand transport, Fig. (2.4), based on the longshore current analysis by Longuet-Higgins (1970). The distribution shows the maximum longshore current at approximately ($x/x_b = 0.65$) and the maximum longshore sand transport at approximately ($x/x_b = 0.80$).

Sawaragi and Deguchi (1979) utilized circular bed load traps which enable them to measure the on-offshore sand

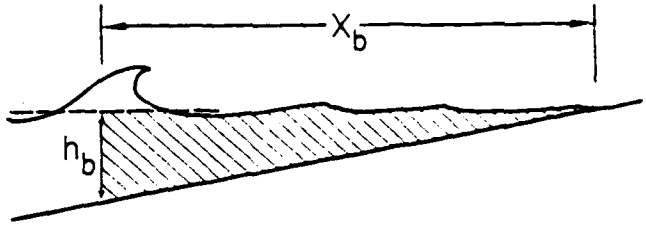

Figure (2.3). Schematic of defining the location and the water depth at the breaker line X_b and h_b.

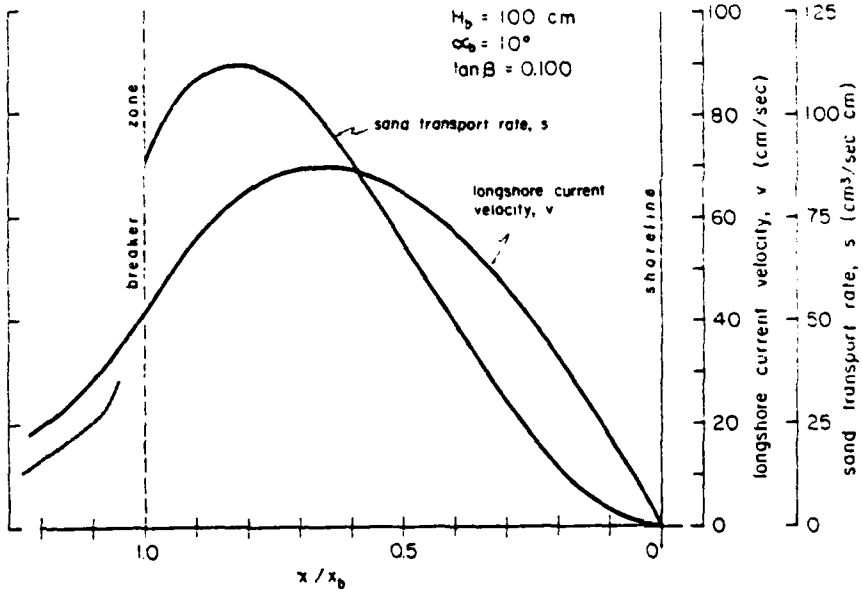

Figure (2.4). Longshore current and sand transport distributions determined by Komar (1977a). [from Komar (1977a)]

movements as well as the longshore transport distribution across the surf zone. The results showed sediment transport to be relatively independent of wave steepness H_o/L_o, but dependent on the sand grain size. The maximum sand transport is shown (Fig. 2.5) to occur at approximately $(x/x_b = 0.6)$ and maximum longshore current at $(x/x_b = 0.4)$.

Bailard (1982) extended his earlier work in which he used second order Stokes theory to describe the wave motion. He included the Ostenddorf and Madsen (1979) longshore current model to predict the distribution of sediment transport rate for different ratios of the velocity of the flow to the sediment fall velocity (Fig. 2.6). He finds the maximum longshore current at approximately $(x/x_b = 0.6)$ with the maximum longshore sand transport at $(x/x_b = 0.9)$.

Results from different studies examining the longshore current and longshore sand transport distributions are given in Table I.

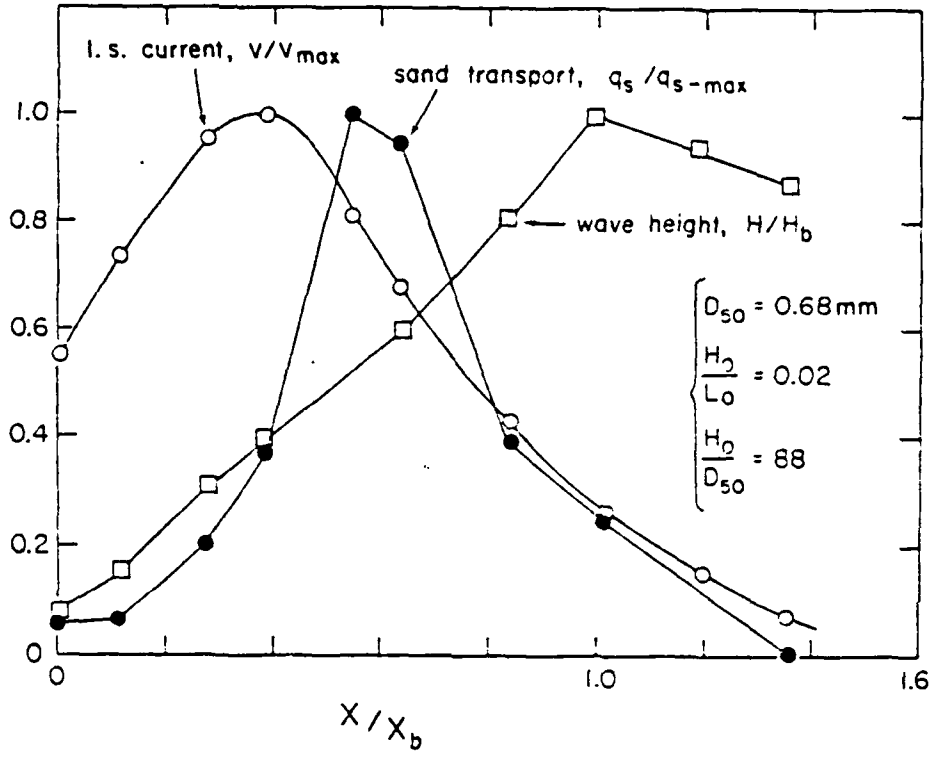

Figure (2.5). Laboratory measurements of the distribution of the longshore current and the sand transport rate showing the positions of the maximum sand transport and maximum longshore current relative to the breaker zone. [based on data of Sawaragi and Deguchi (1979)]

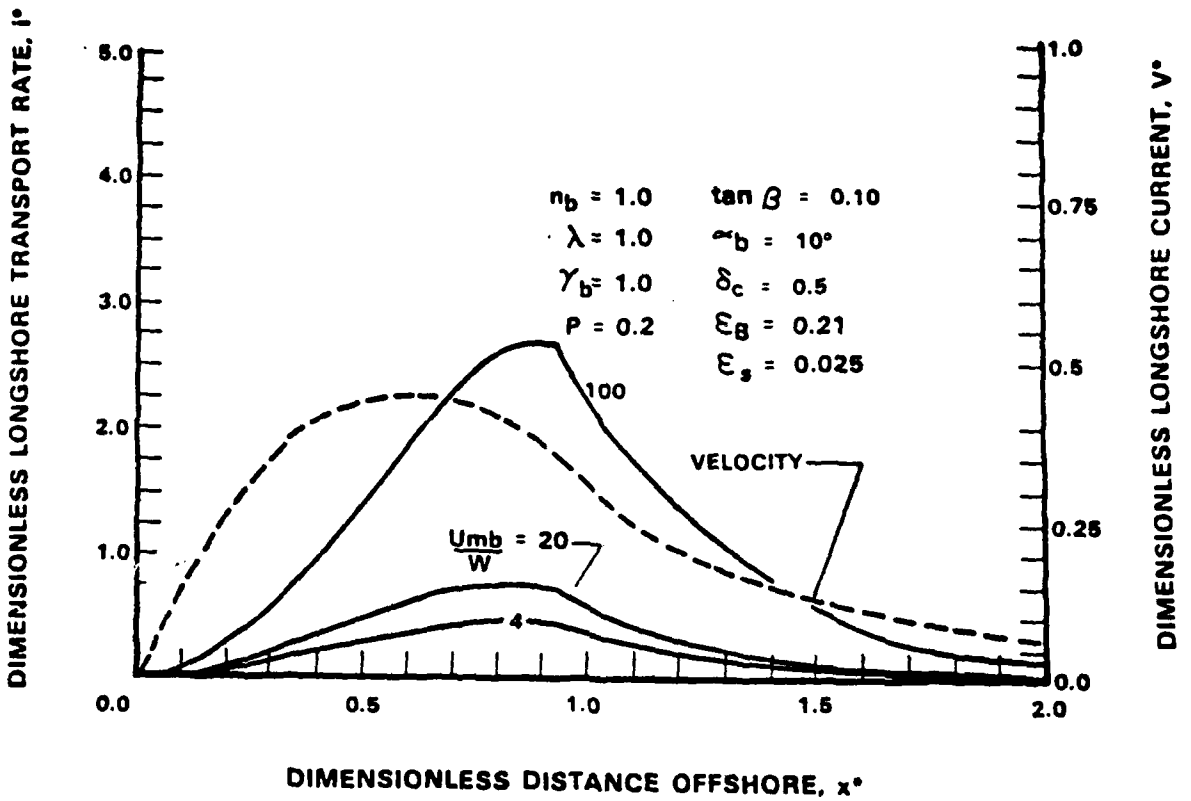

Figure (2.6). Sediment transport and velocity profiles for different values of the velocity ratio $\frac{u_{mb}}{w}$, where u_{mb} is the oscillating water velocity magnitude at the breaker line and w is the sediment fall velocity. [from Bailard, 1982]

TABLE I

Location of Maximum Longshore Current (v/v_{max}) and Longshore Sand Transport (q/q_{max}) Distributions From Different Models

Model and Year	x/x_b		Remarks
	v/v_{max}	q/q_{max}	
Thornton (1973)	-	1.0	Field data and theoretical relationship (2.11) with $B_s = 0.08$
Komar (1977a)	0.65	0.80	Theoretical relationships (2.5), (2.12)
Sawaragi and Deguchi (1979)	0.40	0.60	Laboratory measurements
Bailard (1982)	0.60	0.90	Theoretical relationships

III. DESCRIPTION OF LEADBETTER BEACH EXPERIMENT, SANTA BARBARA, CALIFORNIA

A. GENERAL

Leadbetter Beach, Santa Barbara, California was chosen as the second NSTS experimental site, after Torrey Pines Beach, California, primarily because it is adjacent to a total sand trap forming a spit off the Santa Barbara breakwater, and because it has relatively straight and parallel nearshore depth contours. The NSTS Santa Barbara experiment began in October, 1979 with a 14-month sediment trap study measuring sand accumulation, coupled with a one-month intensive experiment during 27 January through 25 February 1980.

Exceptional storms were encountered towards the latter part of the intensive experiment. During the period 16-20 February 1980, the weather conditions deteriorated greatly approaching the 50-year storm. Significant wave heights in excess of 2 meters and longshore current speeds of 150 cm/sec were recorded. These conditions coupled with spring tides, high winds and wave set-up, eroded the foreshore and back beach areas approximately 2 meters in elevation. These phenomena coupled with high quality data, make the Santa Barbara experiment very unique and significant for near-shore transport studies (Gable, 1981). This study emphasizes the very intensive storm period of 17-18 February, 1980.

B. COASTAL GEOMORPHOLOGY

The shoreline between Point Conception and Santa Barbara has the unusual (for the California Coast) east-west orientation on a predominantly north-south coast. The coastal areas of Santa Barbara are composed of marine sedimentary rock and Monterey Shale-bluffs 30 m high fronted by sand and cobble beaches varying from 0 to 30 m in width (Corps of Engineers, 1970). The major sources of sand for the Santa Barbara beaches are the Santa Maria and Santa Ynez rivers (see Fig. 3.1). Some sand comes from the erosion of the coastal cliffs (Trask, 1952). Bascom (1951) suggests some contribution by wind blown sand, but neither of these two sources are relatively important. Textural analysis of the sands indicates the beaches are composed of fine to medium grain size and are relatively well sorted with a mean diameter of 0.236 mm.

C. WEATHER

The climate in the Santa Barbara area is classified as a Mediterranean type and characterized by warm, dry summers and mild, wet winters. The summers are mostly dry because a semi-permanent high pressure area covers the Eastern North Pacific Ocean, which deflects eastward storms to the north. During winters, this Pacific high migrates southward and weakens, allowing occasional frontal systems to move through Southern California.

The prevailing winds for the West Coast are from the northwest due to the semi-permanent Pacific high pressure and

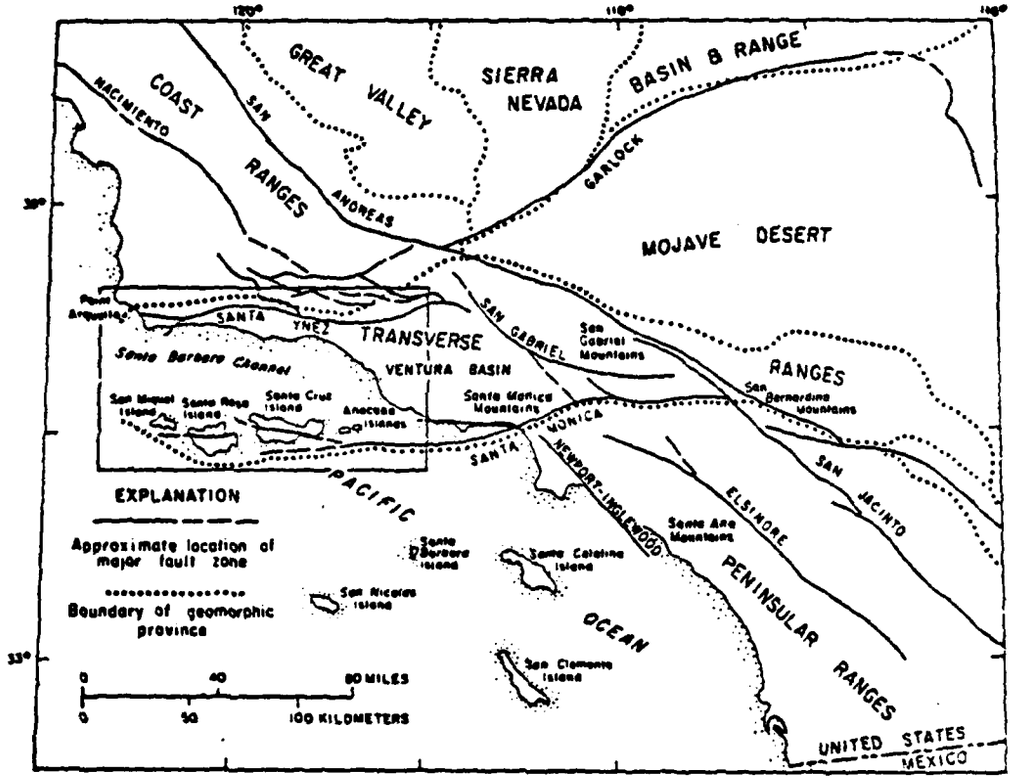

Figure (3.1). Location of Santa Barbara Channel (USGS, 1976).

blow generally parallel to the coastline. However, due to the orientation of the coastline at Santa Barbara and the protection from Point Conception, the winds are generally light and variable from the southerly direction. The average wind speed is less than 3 m/sec and the typical pattern is that of a breeze.

Most extratropical winter storms that affect the Santa Barbara area move southeastward from the Northeast Pacific; on the average, 1 or 2 such storms influence the Santa Barbara channel region every year.

In February 1980, the Eastern Pacific high pressure system was weaker than normal and displaced southeast of its normal position. At the same time, the low pressure center was also displaced south of its normal position. The surface pressures were as much as 18 millibars below normal east of the low center. The Eastern Pacific high pressure system was almost non-existent, which shifted the storm track sufficiently to bring storms onshore in Central and Southern California (Miller, 1980).

Two series of frontal systems hit the study site. A strong southeasterly occurred from 13 to 16 February and a very intensive southwesterly from 17 through 21 February. Because these storms were southerly, they produced large westerly ocean swells and waves which moved into the Santa Barbara channel. The relatively warm water was a major factor which intensified the storm and brought much heavier rain

than normal. Precipitation was 13.2 cm above normal at this time of the year. All these factors, coupled with extreme high tides and wave height, caused extreme beach erosion.

D. WAVES AND WIND CLIMATE

The wave climate at the experimental site is either locally generated inside the Channel Islands or propagated from the open ocean. Normally, the predominant waves are swell from the west-southwest and the west (240°-270° true) entering through a narrow window between San Miguel Island and Point Conception with an average wave height of 91 cm and an average wave period of 12 seconds (Weigel, 1950). The waves must refract almost 90° to reach Leadbetter Beach (Fig. 3.2). As a consequence, the swell waves reaching Santa Barbara are greatly reduced in height and arrive at large angles due to the severe refraction (O'Brien, 1950).

As a result of the origin of the waves, the offshore islands, and the refraction of the waves, the wave pattern in Santa Barbara is nearly the same for all times of the year, with the exception of the waves from the occasional southeast storms. The swell from the open ocean, refracting and breaking at high angle of incidence, create a strong easterly longshore current. The occasional southeasterly storms also create reversals where the longshore current is to the west.

The local wind waves from the south are usually insignificant with only choppy seas and small waves. The local storms

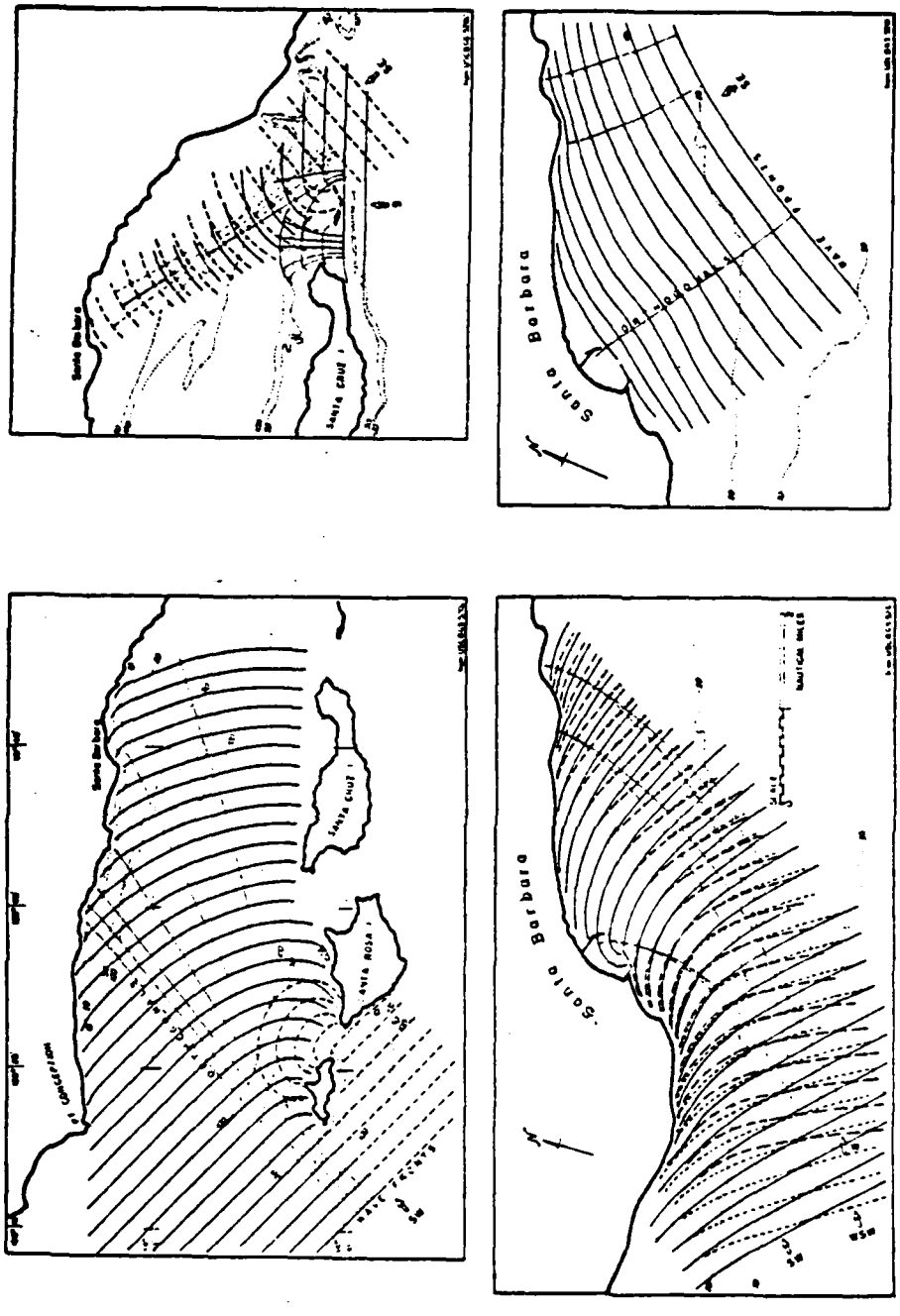

Figure (3.2). Refraction diagrams for Santa Barbara and vicinity for waves of 10-second period: (a) waves from the southwest; (b) waves from the south and southeast; (c) expanded refraction drawing, waves from the west, west-southwest, and southwest; (d) expanded refraction drawing, waves from the southeast (after O'Brien, 1950).

from the southeast (125°-145° true) have a maximum fetch of 145 Km and can propagate waves toward the Santa Barbara Coast with significant wave height ranging up to 488 cm (Weigel, 1950). During the storm period (16-20 February, 1980), waves generated thousands of kilometers away with unlimited fetch were funneled through the wave window of (240°-270° true). The wave period was 14-16 sec with significant wave height approaching 200 cm from the southwest and west. The significant wave height was 190 cm from the southeast on February 16 and 185 cm from the west on February 20, 1980.

E. EXPERIMENT

The start of the experiment was timed such that a strong negative low tide occurred during the daylight hours allowing nearshore instruments to be installed on a dry beach. The tides are semidiurnal with a mean range of 110 cm referred to mean lower low water. The tides ranged from -10 cm to +200 cm (MLLW) during the intensive experiment.

A plan view of Leadbetter Beach (Fig. 3.3) shows the location of the instruments, the experiment baseline and the five range lines. It is noted that the five range lines are not equally spaced.

Series of current meters, pressure sensors and run-up meters were used to measure the wave characteristics during shoaling, breaking, and run-up. The location of the two wave slope arrays is shown in (Fig. 3.4).

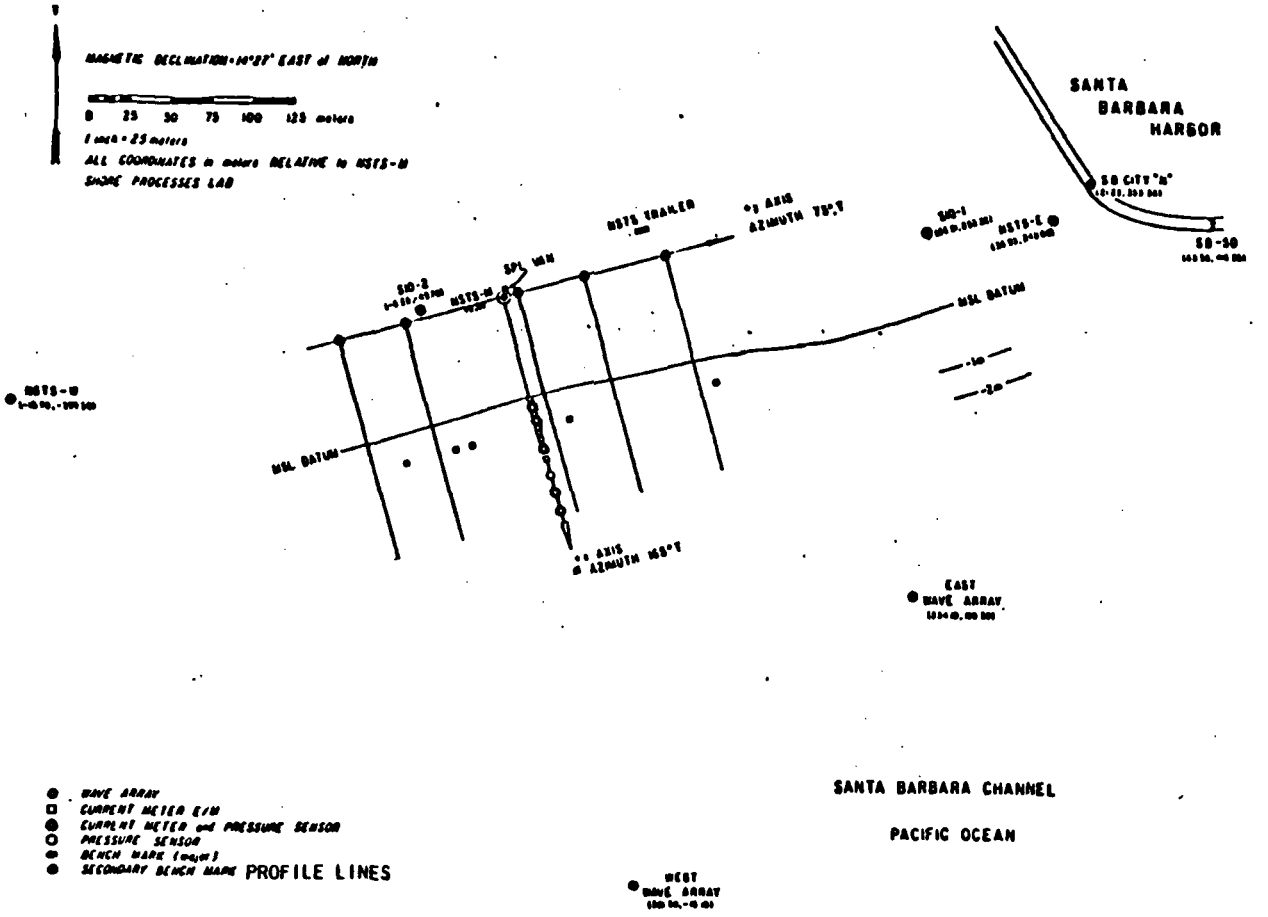

Figure (3.3). Plan view of the study site showing the experimental baseline and the five ranges.

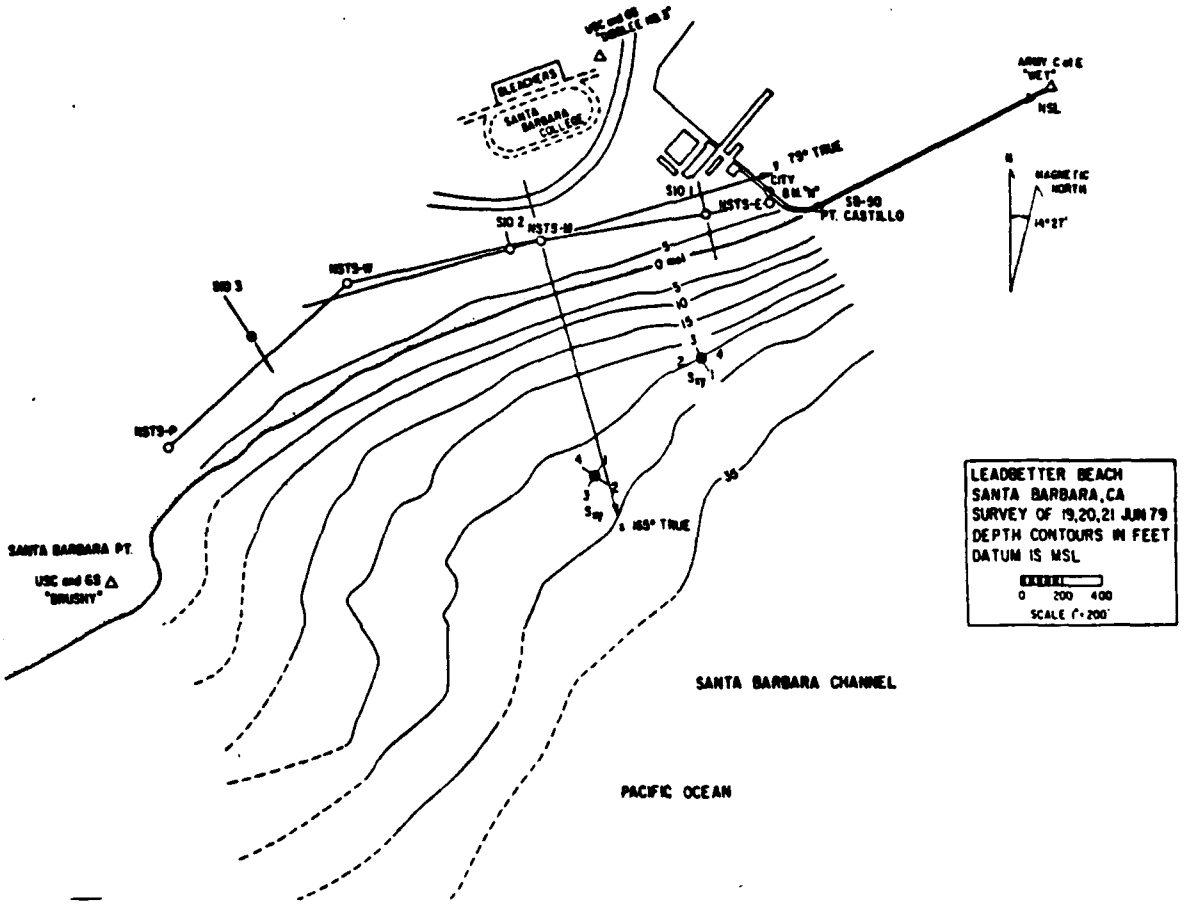

Figure (3.4). Location of the two S_{xy} pressure sensor arrays.

1. Incident Wave Field Measurements

Two, 6 meter square arrays, composed of four Kulite solid state pressure sensors were used to measure an unbiased estimate of the spectrum of the radiation stress, S_{xy}. The square arrays are less efficient than a linear array in estimating a complete directional spectrum but the narrow wave window provided by the offshore islands of Santa Barbara Beach produces an acceptable wave climate estimate. The location and orientation of the two slope arrays are shown in Fig. (3.4). The water depth at both arrays is approximately 9 m and the sensors were mounted 120 cm above the bottom.

2. Profile Measurements

Profile measurements at Santa Barbara consisted of daily wading profiles of the beach face and shallow nearshore, coupled with offshore surveys to a depth of 4 m using a tractor and boat survey for pre- and post-experiment measurements to 12 m depth. Five range lines, extending essentially perpendicular to the beach and covering 200 m alongshore, were established for the daily wading profile (Fig. 3.3). The offshore distances along range lines are referenced to the distance from the experimental baseline (y-axis).

The wading profiles were done using conventional rod and level survey techniques on a daily basis. Range lines were defined by two survey points marked by flags, which a rodman aligned before each survey reading. Rod stations were measured using a specially constructed plastic-coated steel survey line marked at 5 m intervals. An engineer's level and

rod provided vertical control. The profile survey was terminated when the water became too deep for the rodman, or the breaking waves made it impossible to plumb the rod. These surveys were completed at the lowest possible tides occurring during daylight hours. Each survey was closed to the original benchmark on land to verify survey accuracy. Data were entered on site by hand into a Tektronix computer terminal within a short time after each survey. Profiles were plotted immediately to visually search for errors which were due to either data entry or a bad survey point which could be corrected by redoing the field survey immediately.

Generally, small scale changes occurred in the profile during most of the intensive month-long experiment (Fig. 3.5), except during the storm where the beach was cut vertically 2.5 m and horizontally about 60 m within almost a four day period. Although it was impossible to maintain the nearshore instrumentation during the storm, the deep water instruments continued to work, providing an extremely valuable data set on beach erosion.

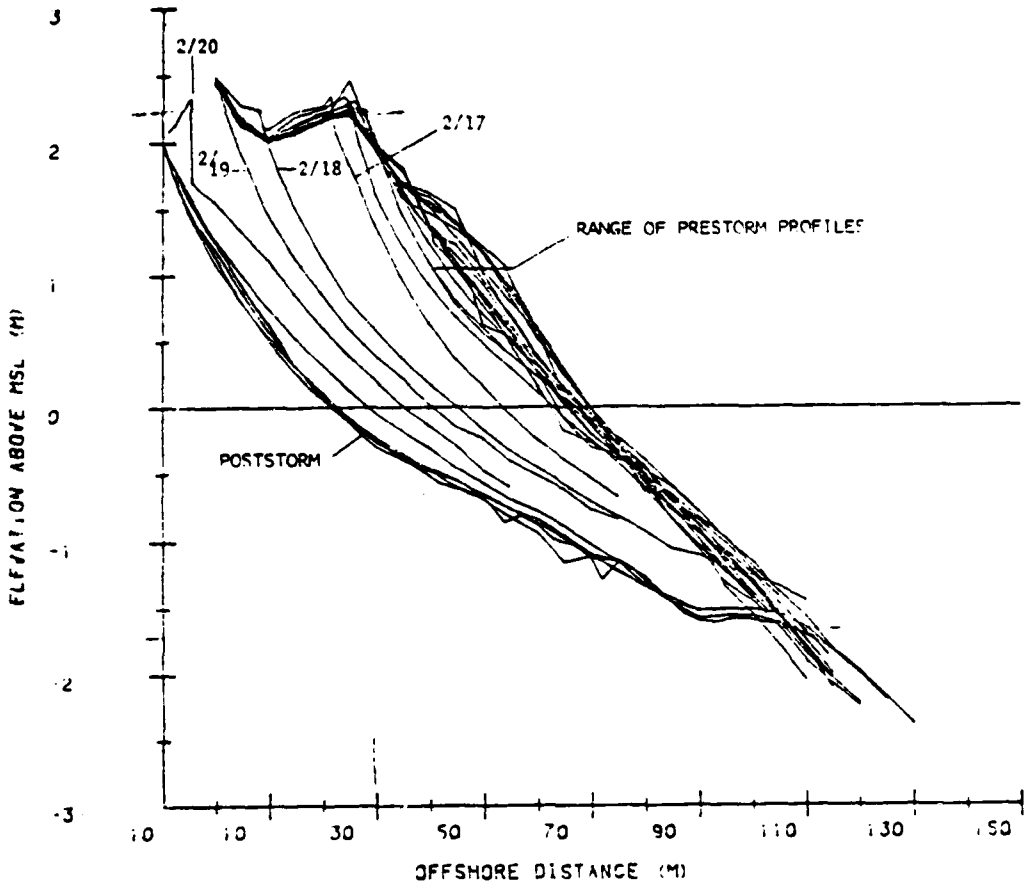

Figure (3.5). Beach profile time history.

IV. FIELD DATA ANALYSIS

A. BEACH PROFILES AND CONSERVATION OF SAND TRANSPORT EQUATION

Five beach normal ranges at Leadbetter Beach were surveyed on a daily basis starting from the established baseline on the beach to a distance about 100 m offshore. Standard rod and level technique described in (III.E.b) were used. Data from the boat-fathometer survey conducted on 25 February, 1980 for the five ranges were used to extend each profile out to the shallow water limit at x = 180 m where $(\frac{h}{L} \leq \frac{1}{20})$.

Linear interpolation was applied twice, first to calculate the missing data points, and second to define five equally spaced ranges (50 m apart). The five ranges were averaged for both 17th and 18th of February to produce a daily mean profile. Then, a "mean beach" profile was defined by averaging these two daily profiles. Fig. (4.1) shows the mean beach profile, relative to mean sea level (MSL) and indicates no well developed bar structures or trough along the profile.

Based on the difference in elevations between the 17th and 18th February surveys at each location, the net longshore transport distribution is calculated using the conservation analysis of sand transport described later in this section. A "mean net longshore transport", $\bar{q}_{mean}$, distribution was obtained by averaging the net transport distributions for the five ranges. The "mean net sand transport" distribution and

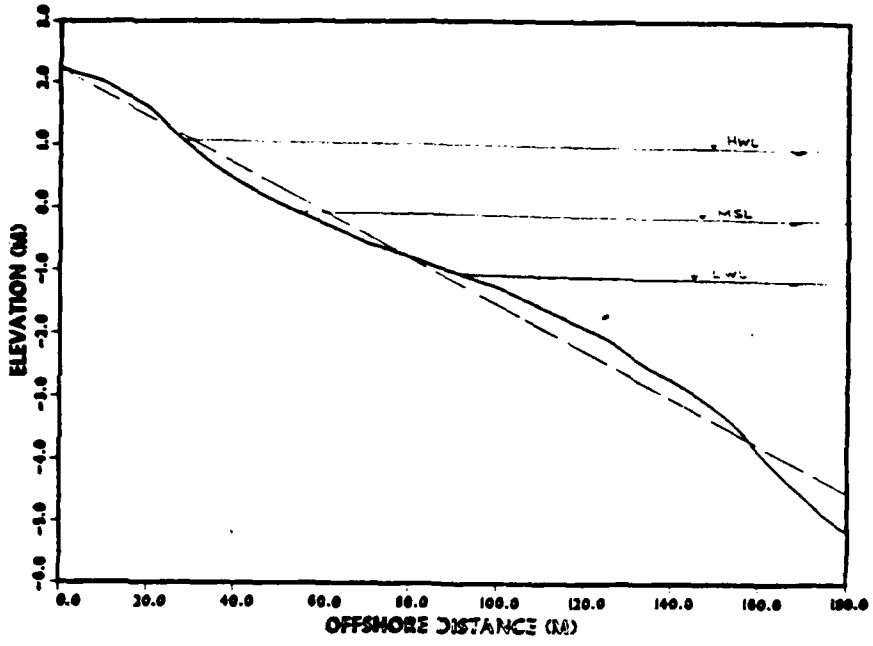

Figure (4.1). Mean beach profile gives an average profile slope of 0.037 relative to HWL, LWL and MSL.

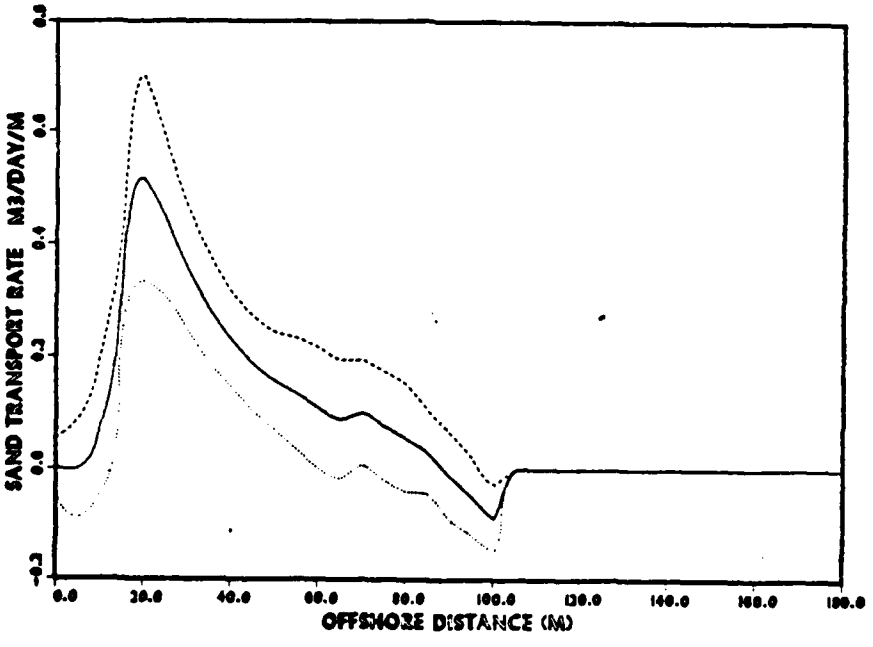

Figure (4.2). Sand transport distribution inferred from the field data based on the profile changes showing a maximum transport at the beach face.

the standard deviation calculated at each point are shown in Fig. 4.2 indicating a small variance with acceptable scatter around the $\bar{q}_{mean}$ distribution.

The $\bar{q}_{mean}$ distribution goes to zero after a distance of 100 m offshore as shown in Fig. 4.2 because the wading profiles on the 17th and 18th are extended after this distance by the same fathometer data taken on 25 February.

Profile changes between sequential measurements can be approximated by a parallelopiped with sides Δx, Δy and the time varying depth (Δh). Considering the equilibrium of the parallelopiped element (Fig. 4.3), the net sand trnasport rate in the x-direction is $q_{x\,net}\,\Delta y = \frac{\partial q_x}{\partial x}\Delta x\Delta y$ and the net sand transport rate in the y-direction is $q_{y\,net}\,\Delta x = \frac{\partial q_y}{\partial y}\Delta y\Delta x$. The total net sand transport rate ($q_{x\,net}\,\Delta y + q_{y\,net}\,\Delta x$) is balanced by the rate of the net volume changes over the element giving

$$q_{x\,net}\,\Delta y + q_{y\,net}\,\Delta x = (1-a)\,\frac{\Delta h}{\Delta t}\,\Delta x\Delta y \qquad (4.1)$$

where a is the sand porosity and is taken as 0.40. Equation (4.1) can be written as

$$\frac{\partial q_x}{\partial x} + \frac{\partial q_y}{\partial y} = (1-a)\,\frac{\partial h}{\partial t} \qquad (4.2)$$

Since a strong longshore current was observed during 17 and 18 February, (see Fig. (6.3)), a significant longshore

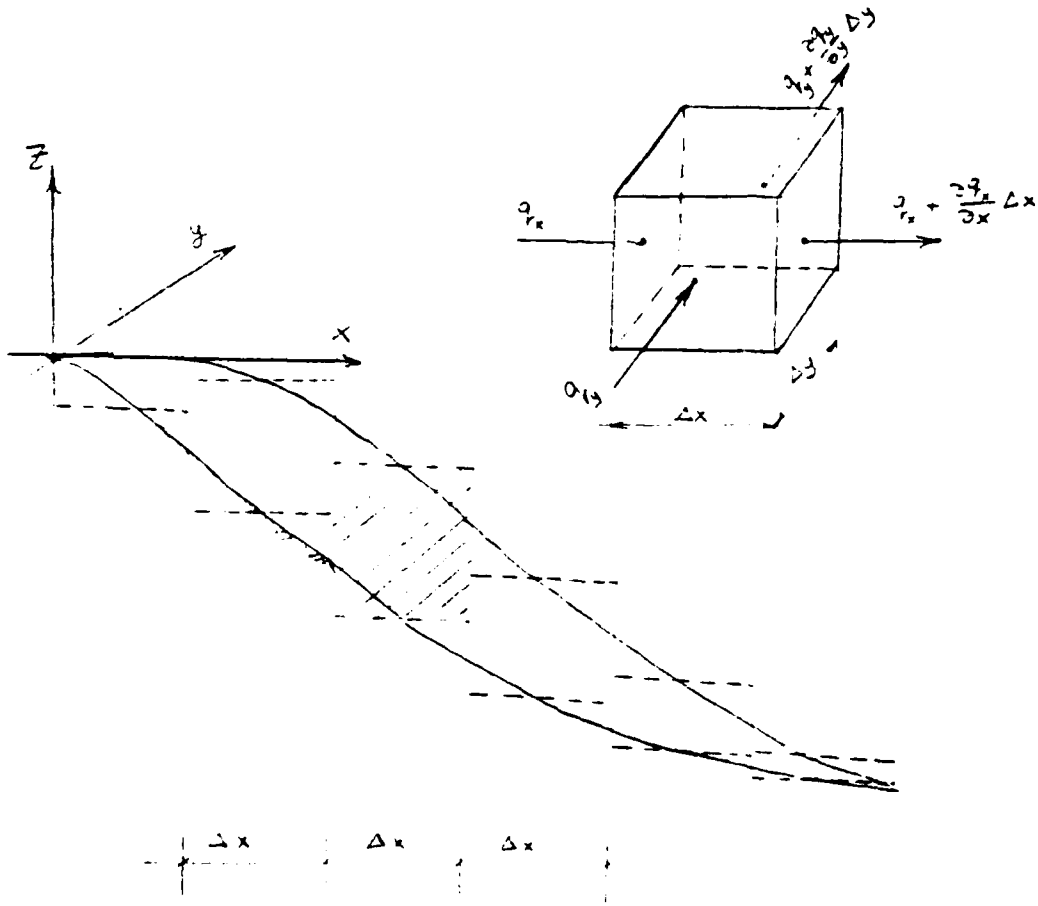

Figure (4.3). Conservation of sand transport with changes in the beach profile.

sand transport was expected. Therefore, it is hypothesized that the longshore sand transport is much larger than the on-offshore sand transport, i.e., $q_y >> q_x$. The profile changes *in Fig. 3.6 do not show any* well-defined bar or trough structures which suggests the on-offshore sand transport is negligible (i.e., $\frac{\partial q_x}{\partial x} = 0$). Thus, equation (4.2) becomes

$$\frac{\partial q_y}{\partial y} = (1-a) \frac{\partial h}{\partial t} \qquad (4.3)$$

Equation (4.3) states simply that the changes in the beach profile with respect to time, are proportional to the net longshore sand transport. The transport rate/unit width of on-offshore distance, q_y, can be calculated since water depth (h) is measured as a function of time (t). The boundary conditions are needed to solve (4.3). For the offshore boundary condition it is assumed

$$q_y = 0 \quad \text{at} \quad h = h_o$$

where h_o is the water depth at the shallow water limit, $h_o = \frac{L}{20}$, and L is the wavelength. Given the dominant wave period of 14 sec (f_p = 0.0703 Hz), h_o was calculated to be 5.0 m at a distance approximately 180 m from the baseline. The nearshore boundary condition requires the sand transport to go to zero at the shoreline. It appears from Fig. 4.2 that this condition is satisfied from the data at the baseline at x = 0. The net sediment transport rate is calculated by

integrating the net cross-shore distribution which is assumed to be similar to the longshore sand transport distribution.

For discussion purposes, two regions within the surf zone are defined. A swash region is defined from the baseline to the intersection of HWL with the profile, i.e., (from x = 0 to x ≃ 30 m); a seaward region is defined from x ≃ 30 m to x ≃ 180 m. The swash region indicates significant erosion on the beach face (Fig. 4.2), which will not be considered in this study because the model does not include sediment transport on the beach face. The seaward region shows the eroded profile with a small accreted area around x = 90 m, which appears with a negative sign.

B. RADIATION STRESS, WAVE HEIGHT AND DIRECTION AT OUTER BOUNDARY

Measurements from a 610 cm square, four pressure sensor array in 8-m water depth are used to produce an unbiased estimate of the spectrum of radiation stress. The pressure arrays worked throughout the experiment including the storm period. The array measurements are also used to calculate the height and the directional characteristics of the waves. The radiation stress (S_{xy}) is given by (Longuet-Higgins, 1962)

$$S_{xy} = \overline{\int_{-h}^{\eta} \rho u_w(z,t)\, v_w(z,t)\, dz} \qquad (4.4)$$

where u_w and v_w are the crossshore and alongshore components

of wave velocity. The velocities are calculated from the pressure gradients measured at the array applying linear wave theory spectral transformations. For a particular component

$$u_j(f,z,t) = \frac{1}{\omega}\left[\frac{i \cosh k(h+z)}{\rho \cosh k(h+z_m)}\right] \frac{\partial p}{\partial x_j}, \quad j = 1,2 \qquad (4.5)$$

where the z_m is the measured depth of the pressure sensors, ω is the radial frequency and j refers to the two horizontal components. The term between the brackets is the spectral transfer function H(f) relating the measured pressure gradients to inferred velocity components. Substituting equation (4.5) into (4.4), using the measured pressure head $\frac{p}{\rho g}$ and integrating

$$S_{xy}(f) = \left[\frac{\rho g^2}{2 \omega^2 k(\cosh^2 k(h+z_m))}\right] C_{\frac{\partial p}{\partial x},\frac{\partial p}{\partial y}}(f) \qquad (4.6)$$

where $C_{\frac{\partial p}{\partial x},\frac{\partial p}{\partial y}}(f)$ is the co-spectrum between the measured pressure gradient components.

Wave heights were determined from the surface elevation records using the "zero-up-crossing method" in which the wave height is defined as the difference between the maximum and minimum occurring between two consecutive zero-up-crossings. Surface elevation records were first linearly detrended to exclude the effects of the rising and falling of the tides and then high-pass filtered with a cut-off frequency of 0.05 Hz to exclude surf beat, followed by a low-pass filter with a high frequency cut-off (0.3 Hz).

The filtering was accomplished by Fourier transforming the signals, zeroing the Fourier amplitude coefficients in the filtered frequencies, and inverse transforming the complex spectrum to obtain the filtered time series. The entire 68-minute-record was transformed at one time to minimize the end effects which result in spectral leakage, and to obtain maximum resolution giving very sharp roll-off at the filter cut-offs.

Due to the large number of current meters, current data are utilized applying linear theory to infer wave heights from the velocities (Guza and Thornton, 1980). Surface elevation time series were obtained from current measurements using the complex Fourier spectra of the horizontal velocity component U(f), V(f). The complex surface elevation spectrum, X(f), is calculated applying the linear wave transfer function, $\vec{H}(f)$

$$X(f) = \vec{H}(f) \cdot \vec{V}(f) \qquad (4.7)$$

Then, the complex surface elevation spectrum is inverse transformed to obtain the surface elevation time series from which the wave height distribution is calculated. Surface elevations were also inferred from pressure signals in a similar manner by transforming the pressure records using linear theory.

A mean incident wave angle ($\bar{\alpha}$) and a representative frequency (f_p) are defined for input into the models such that

using $\bar{\alpha}$ and f_p to calculate the total radiation stress S_{xy}^T, the same value is obtained as that measured by the pressure sensor array.

The radiation stress (S_{xy}) in equation (4.4) can be expressed applying linear wave theory for long-crested waves

$$S_{xy}(f) = E(f)\, n(f) \sin\alpha \cos\alpha \qquad (4.8)$$

The total radiation stress (S_{xy}^T) is calculated using

$$S_{xy}^T = \int S_{xy}(f)\, df \qquad (4.9)$$

Then, the calculated S_{xy}^T is equated to its equivalent S_{xy}^T in (4.8) for monochromatic ($f \approx f_p$) waves approaching at a mean angle $\bar{\alpha}$

$$S_{xy}^T = E^T n(f_p) \sin\bar{\alpha}(f_p) \cos\bar{\alpha}(f_p) \qquad (4.10)$$

where E^T is the total energy. Applying linear theory relationships a mean incident wave angle $\bar{\alpha}$ is defined as:

$$\bar{\alpha}(f_p) = \frac{1}{2} \sin^{-1} \left(\frac{2S_{xy}^T}{E^T(f_p) n(f_p)} \right) \qquad (4.11)$$

where the representative frequency f_p is the peak frequency of the energy spectrum. Since the radiation stress is calculated using the pressure gradients, the kinetic energy calculated

using the pressure gradient is introduced for consistency of the analysis. It is assumed the kinetic energy E_k is half the total energy. Then equation (4.11) yields

$$\bar{\alpha}(f_p) = \frac{1}{2}\sin^{-1}\left\{\frac{S^T_{xy}}{E_k n(f_p)}\right\} \tag{4.12}$$

The kinetic energy is calculated using the pressure gradient component spectrum

$$E_k(f) = |H(f)|^2[G_{\frac{\partial p}{\partial x}}(f) + G_{\frac{\partial p}{\partial y}}(f)] \tag{4.13}$$

where $|H(f)|^2$ is the linear wave transformation function given by

$$|H(f)|^2 = \frac{\rho g^2}{4k\omega^2}\frac{sinh(2kh)}{\cosh^2 k(h + z_m)} \tag{4.14}$$

The mean incident wave angle ($\bar{\alpha}$) at the pressure sensor's location was then refracted shoreward to the 5 m contour (at the shallow water limit). A refraction calculation was performed over a bathymetric chart of the experimental site that shows the beach has straight and parallel contours shoreward of 5 m depth (Fig. 4.4). Applying linear refraction to the measured mean angle ($\bar{\alpha}$ = 12.4°) at the pressure sensor location and peak frequency (f_p = 0.07 Hz), waves reach the 5 m contour with a refracted angle $\bar{\alpha}_s$ = 9.0° where the calculated refraction coefficient K_r equals 0.985.

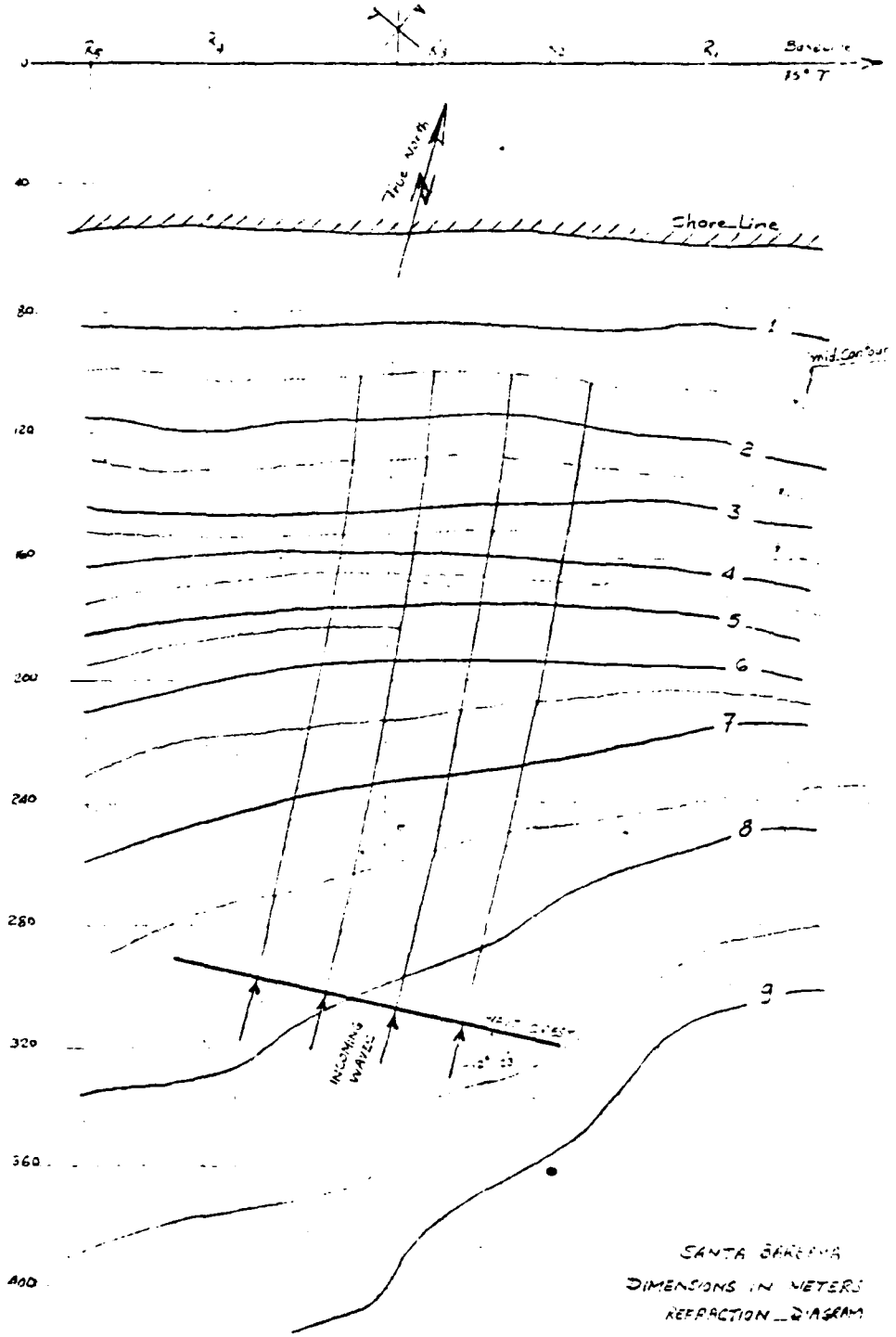

Figure (4.4). Refraction diagram for Santa Barbara (17 February, 1980).

The H_{rms} is calculated using linear refraction theory:

$$\frac{H_{rms}}{H_{rms(8m)}} = \left(\frac{C_{g_{8m}}}{C_g}\right)^{1/2} \left(\frac{b_{8m}}{b}\right)^{1/2}$$

$$= \left(\frac{C_{g_{8m}}}{C_g}\right)^{1/2} (K_r) \qquad (4.15)$$

giving a refracted H_{rms} equivalent to .85 m at water depth h_o = 5 m, which is used as the initial wave height for the model. Refracted wave rays were extended to get the angle of approach at the breaker line calculated to give $\bar{\alpha}_b = 6.0°$. The breaker line was defined at maximum H_{rms}. $\bar{\alpha}_b$ was used to calculate the longshore sand transport using the wave power expression.

Table II gives various calculated parameters of S_{xy}, $\bar{\alpha}$, f_p, H_{rms} at different times before, after and during the 17th and 18th of February. Orientation of the coordinates leads to a negative sign for both S_{xy} and $\bar{\alpha}$, indicating the waves are coming from the west.

TABLE II

Calculated Parameters at West Pressure Sensor
(During 17-18 February)

Date	time	depth (m)	tide (cm)	S_{xy} (Erg/cm^2)	$\bar{\alpha}°$	$\bar{f}_p$ (Hz)	H_{rms} (cm)
17th February 1980	0730	9.2	+71	-0.43×10^5	-5.8	0.094	65.6
	1800	7.8	-71	-1.76×10^5	-12.4	0.070	88.8
	2230	9.4	+86	-2.16×10^5	-13.0	0.062	96.2
18th February 1980	0920	9.5	+96	-2.61×10^5	-15.9	0.070	96.2
	2200	9.2	+74	-1.25×10^5	-15.0	0.094	70.0

V. LONGSHORE SEDIMENT TRANSPORT MODEL

A littoral sand transport model is develcped based on the energetics approach expressed by Thornton (1973) in which the energy transformation is described by the random wave model of Thornton and Guza (1983a) coupled with the longshore current model of Thornton and Guza (1983b). The input to the predictive model are the offshore rms wave height, mean direction and mean period. Both an analytical model for plane sloping beaches and a numerical model for arbitrarily bottom profile are presented.

A. DEVELOPMENT OF SAND TRANSPORT MODEL

Assuming stationary wave conditions with a beach of straight and parallel contours, the gradient of the wave power in the on-offshore direction $\frac{dECg_x}{dx}$ is balanced by the ensemble averaged dissipation due to both wave breaking $\langle \varepsilon_b \rangle$ and bottom friction $\langle \varepsilon_f \rangle$ (Thornton and Guza, 1983) such that

$$\frac{dECg_x}{dx} = \langle \varepsilon_b \rangle + \langle \varepsilon_f \rangle \qquad (5.1)$$

The wave power is expressed using the linear wave theory relationships:

$$E = \frac{1}{8} \rho g H_{rms}^2 = \frac{1}{8} \rho g \int_o^\infty H^2 P(H) \, dH \qquad (5.2)$$

$$Cg_x = \frac{C}{2}\left[1 + \frac{2kh}{\sinh 2kh}\right]\cos\bar{\alpha} \qquad (5.3)$$

where H_{rms} is the root mean square wave height, $\bar{\alpha}$ is the mean wave direction and k is the wavenumber associated with peak frequency f_p.

Dissipation due to wave breaking $\langle\varepsilon_b\rangle$ can be modeled after a periodic bore, applying conservation of mass and momentum at regions of uniform flow up-and-downstream of the bore as shown in Fig. (5.1). The average rate of energy dissipation per unit area for single breaking wave is calculated (Stoker, 1957):

$$\varepsilon_{bore} = \frac{1}{4}\rho g \frac{(h_2 - h_1)^3}{h_1 h_2} Q \simeq \frac{1}{4}\rho g C \frac{H^4}{h^3} \qquad (5.4)$$

where the wave height H is measured as the maximum to minimum of the bore, Q is the volume discharge of flow per unit area across the bore described by simple linear bore theory after Hwang and Divoky (1972), and B is a breaker coefficient of 0(1). The coefficient B is an unspecified parameter in the model, which is determined from the data.

The Rayleigh distribution is assumed to describe the waves everywhere with the implied assumptions that the waves are very narrow band such that they can be described by a single frequency f_p and mean direction $\bar{\alpha}$. Thornton and Guza (1983) predict the fraction waves which are breaking at each location. Using this information, the average rate of energy

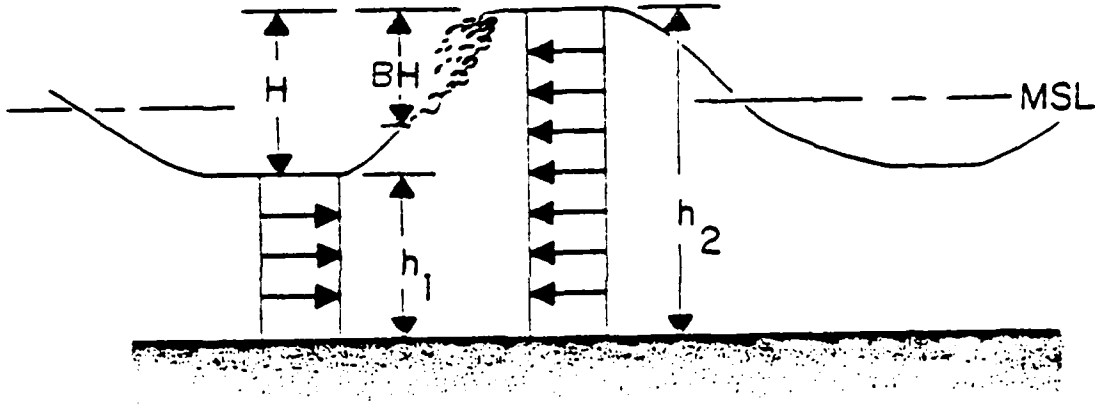

Figure (5.1). Periodic bore used to describe spilling breakers.

dissipation due to breaking $\langle \varepsilon_b \rangle$ is given by

$$\langle \varepsilon_b \rangle = \frac{3\sqrt{\pi}}{16} \rho g \frac{B^3 f_p}{\gamma^4 h^5} H_{rms}^7 , \qquad (5.5)$$

where γ is a coefficient relating H_{rms} to h (taken to be 0.44 by Thornton and Guza, 1983). The average frictional dissipation $\langle \varepsilon_f \rangle$ at the bottom boundary layer for the ensemble (all waves) calculated using Rayleigh probability distribution is:

$$\langle \varepsilon_f \rangle = \frac{\rho C_f}{16\sqrt{\pi}} \left[\frac{2\pi f_p H_{rms}}{\sinh kh}\right]^3 , \qquad (5.6)$$

where C_f is the friction coefficient. Thornton and Guza (1983a) point out that $\langle \varepsilon_f \rangle$ is relatively more important for gently sloping beaches and for low frequency waves, i.e., the shallower the depth the greater the frictional dissipation. They neglect the frictional dissipation as it has a small contribution compared with $\langle \varepsilon_b \rangle$, as will be done here also.

Substituting equations (5.2), (5.3), (5.5), and (5.6) into equation (5.1), yields:

$$\frac{d}{dx} \frac{1}{8} \rho g H_{rms}^2 C_g \cos \bar{\alpha} = \frac{3\sqrt{\pi}}{16} \frac{\rho g f_p B^3}{\gamma^4 h^5} H_{rms}^7 \qquad (5.7)$$

H_{rms} can be evaluated analytically, assuming small incident wave angle ($\cos \bar{\alpha} \simeq 1$) and limiting the analysis to shallow water ($\frac{h}{L} \leq \frac{1}{20}$), which gives

$$H_{rms} = a^{1/5} h^{9/10} [1 - h^{23/4} (\frac{1}{h_o^{23/4}} - \frac{a}{y_o^{5/2}})]^{-1/5} , \qquad (5.8)$$

where

$$y_o = H_o^2 h_o^{1/2}$$

and

$$a = \frac{23}{15} (\frac{g}{\pi})^{1/2} \frac{\gamma^4 \tan \beta}{B^3 f_p} .$$

The value of tan β is the beach slope and the subscript "o" refers to the input conditions at the outer shallow water depth limit. When the water depth gets very shallow, (5.8) becomes

$$H_{rms} = a^{1/5} h^{9/10}; \quad \text{as} \quad h \to 0 , \qquad (5.9)$$

which indicates that the wave height in the inner surf zone is related to the depth and independent of the initial conditions in deeper water.

With the assumptions of straight and parallel depth contours and stationary wave conditions, the longshore current distribution across the surf zone can be estimated using the longshore momentum flux balance (Thornton and Guza, 1983)

$$\frac{\partial S_{xy}}{\partial x} = - \tau_b \qquad (5.10)$$

where τ_b is the bottom shear stress and S_{xy} is the radiation stress defined by Longuet-Higgins and Stewart (1962) (for linear theory) as

$$S_{xy} = E\, C_g \cos\alpha \frac{\sin\alpha}{C}$$

From linear wave refraction

$$\frac{\sin\alpha}{C} = \frac{\sin\alpha_o}{C_o} = \text{constant} .$$

Thus,

$$\frac{\partial S_{xy}}{\partial x} = \frac{\sin\alpha_o}{C_o} \left[\frac{d}{dx} E\, C_g \cos\alpha\right] \tag{5.11}$$

The term in brackets in the R.H.S. is defined in (5.1) as $\langle \varepsilon_b \rangle$. Therefore (5.11) reduces to:

$$\frac{\partial S_{xy}}{\partial x} = \frac{\sin\alpha_o}{C_o} \langle \varepsilon_b \rangle = -\tau_b \tag{5.12}$$

The average alongshore bottom shear stress τ_b is defined by Longuet-Higgins (1970), assuming the quadratic law

$$\vec{\tau}_b = \rho\, c_f \overline{|\vec{u}_t|(V + v_w)\vec{j}} \tag{5.13}$$

where $\vec{u}_t$ is the total instantaneous velocity due to waves and current, V is the longshore current, v_w is the longshore component of the oscillating wave velocity and c_f is the bed

shear stress coefficient. The bar over equation (5.13) indicates averaging in time over one wave period. Assuming a small angle of wave incidence ($\bar{\alpha} < 15°$), and a weak current case following Liu Ph. L-F and R. Dalrymple (1978), equation (5.13) simplifies to

$$\tau_b = \rho\, c_f\, |\bar{u}_w|\, V \tag{5.14}$$

where $\bar{u}_w$ is the mean cross-shore wave velocity.

$|\bar{u}_w|$ is specified using the shallow water wave theory relationships and Rayleigh wave height distribution (Thornton and Guza, 1983) such that:

$$|\bar{u}_w| = \frac{1}{4} \left(\frac{g\pi}{h}\right)^{1/2} H_{rms} \tag{5.15}$$

Substituting (5.11), (5.12), (5.14), (5.15) into (5.10) and solving for the mean longshore current velocity, yields:

$$V = \frac{1}{\rho\, c_f\, |\bar{u}_w|} \frac{\sin \alpha_o}{C_o} \langle \varepsilon_b \rangle$$

$$= \frac{3}{4} \frac{B^3\, f_p\, g^{1/2}}{c_f\, \gamma^4} \frac{\sin \alpha_o}{C_o} \frac{H_{rms}^6}{h^{9/2}} \tag{5.16}$$

The longshore sand transport distribution is obtained by substituting the expressions for the change in energy flux $\left(\frac{\partial EC_g}{\partial x}\right)$, equation (5.1) and the longshore current equation (5.16) into equation (2.11) to give

$$\bar{q}_s = \frac{B_s}{g(1-\frac{\rho}{\rho_s})|\bar{u}_w|}\left\{\frac{1}{\rho c_f}\frac{\sin\alpha_o}{C_o}\right\}^{1/2}\langle\varepsilon_b\rangle^{3/2} \qquad (5.17)$$

Substituting (5.7), (5.15) and (5.16) in equation (5.17) yields:

$$\bar{q}_s = \frac{B_s}{g(1-\frac{\rho}{\rho_s})}\frac{1}{\gamma^6 h^7}\left[\frac{\sin\alpha_o}{C_o}\frac{f_p^3 B^9 H_{rms}^{19}}{c_f}\right]^{1/2} \qquad (5.18)$$

Equation (5.18) has the observed characteristics that outside the surf zone as h reaches h_o, $\bar{q}_s(x)$ gets small and when h goes to zero at the shoreline, $\bar{q}_s(x)$ approaches zero. A maximum transport occurs between these two boundaries.

For a planar sloping beach, the analytical solution for H_{rms} (5.8), which is limited to shallow water, is substituted into (5.18) to obtain the cross-shore transport distribution. For arbitrary bottom profiles (but straight and parallel depth contours), a simple forward differencing scheme is used to numerically integrate equation (5.1) for H_{rms}. The calculated H_{rms} value is substituted into (5.18). The energy flux balance is also numerically integrated from initial offshore distance (at depth h_o) to the shoreline with a spatial interval Δx

$$E\,Cg_x|_{i+1} = E\,Cg_x|_i - \Delta x\left\{\langle\varepsilon_b\rangle|_i + \langle\varepsilon_f\rangle|_i\right\} \qquad (5.19)$$

$$i = 1,2,\ldots,n$$

Equation (5.19) starts at the initial offshore distance (i = 1) where H_o, h_o, f_p, $\bar{\alpha}_o$ are given. The model calculates the forward step by subtracting the total dissipation from the calculated energy flux evaluated from the previous step. The model predicts H_{rms} each step, using linear theory relationships (5.2) and (5.3) until i approaches n at the shoreline. Then, the predicted H_{rms} values are used to calculate the longshore current using (5.16). The sand transport distribution is evaluated using (5.18).

Integrating $\bar{q}_s$ in (5.18) over limits of offshore distances for the study zone, the volume transport rate (Q_ℓ) is calculated as

$$Q_\ell = \int_o^{x_o} \bar{q}_s \, dx \qquad (5.20)$$

where x_o is the offshore distance at which the initial conditions of waveheight (H_o) and water depth (h_o) are given. The coefficient B_s in (5.18) is used to calibrate the model.

VI. MODEL RESULTS AND COMPARISON WITH PROTOTYPE DATA

A. MODEL RESULTS FOR H_{rms} AND V

Field data for the Santa Barbara experiment are utilized to calculate the parameters S_{xy}, $\bar{\alpha}_o$, f_p and H_{rms} which in turn are used as input for both the expressions (5.8) and (5.19). Model coefficients γ, B and c_f were determined from the data. The ratio, $\gamma = \frac{H_{rms}}{h}$ was found to be 0.44 from the slope of the h vs. H_{rms} curve, Fig. (6.1), in the inner surf zone. This agrees with the value reported earlier by Thornton and Guza (1983) for the Torrey Pines Beach experiment.

H_{rms} values inferred from the pressure and velocity measurements at time 1800 on the 17th of February are compared with the wave transformation model for various breaker coefficients, B. Using an iterative scheme, based on the least squares error criterion, B equal to 1.1 gave the best fit to H_{rms} data (Fig. 6.2a). To check on the generality of the model, the waveheight transformation model was run for 5 February using B = 1.1. It also gave the best model fit to the data (Fig. 6.2b).

An optimal bed shear stress coefficient, c_f, was calculated comparing the longshore current model with the measured longshore current values, V. Since there are only three longshore current measurements available on 17 February due to the destruction of instruments by the storm, the data from 5 February were again used. With B = 1.1, c_f was varied to

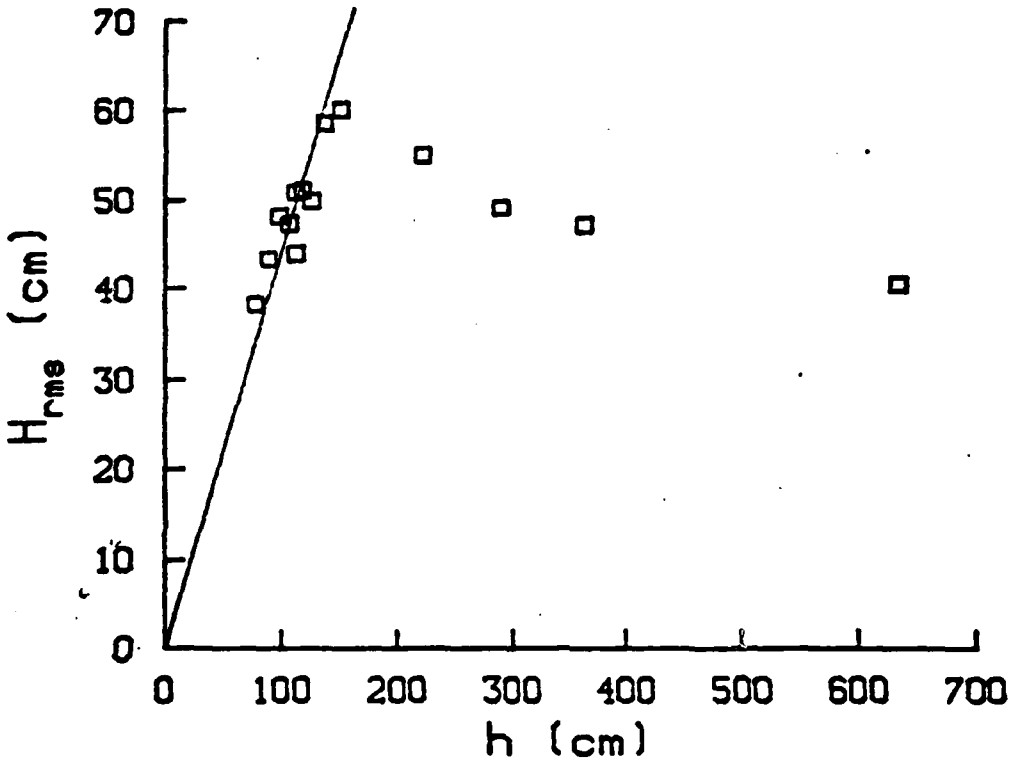

Figure (6.1). Root mean square waveheight vs. water depth for 5 February, 1980, giving $\gamma = 0.44$ in the inner surf zone.

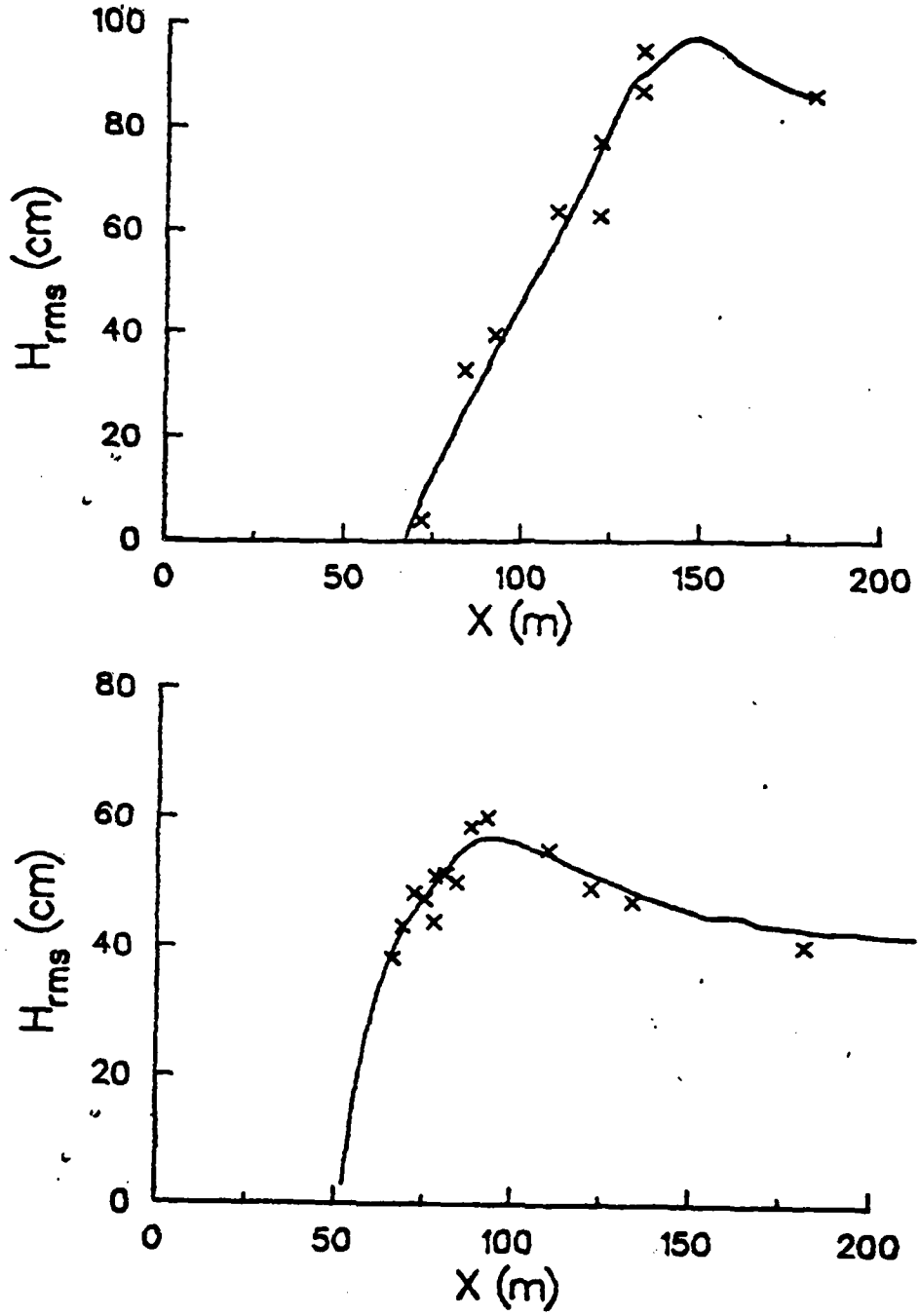

Figure (6.2). Model H_{rms} as a function of offshore distance compared with measurements indicated by x. The model is applied to data; (a) on 17 February; (b) on 5 February, to obtain B which was found to be 1.1 in both days.

obtain the best fit to the measured V. A value of $c_f = 0.005$ gave the best fit (Fig. 6.3b).

B. MODEL RESULTS FOR CROSS-SHORE SAND TRANSPORT DISTRIBUTION

The empirical coefficient B_s in equation (5.18) is used to calibrate the model and will be explained later. In all the calculations and figures, the offshore distance (x) is measured starting from the experimental baseline at x = 0. The average net transport between profiles on 17 and 18 February are to be determined. A weighted time difference of 25 hours was found between the two mean profile surveys.

The model predictions of H_{rms}, V and $\bar{q}_s$ at each x-location depend mainly on the water depth (h). Therefore, two cases are considered to test the sensitivity of the models to the variations in the water depth. In the first case, the water depth does not vary with time. In the second case, the water depth varies by hourly time increments according to tidal variation.

1. Model Results for Constant Water Depth

In this case study, the water depths are held constant at relative MSL. The numerical model utilizes the actual bottom and predicts H_{rms}, V and $\bar{q}_s$. The model results are summarized in Fig. 6.4 indicating the capability of the model to predict the increase in waveheight due to shoaling and the decrease due to breaking processes. The longshore sand transport and the longshore current have a similar distribution, which implies that the sand transport may primarily

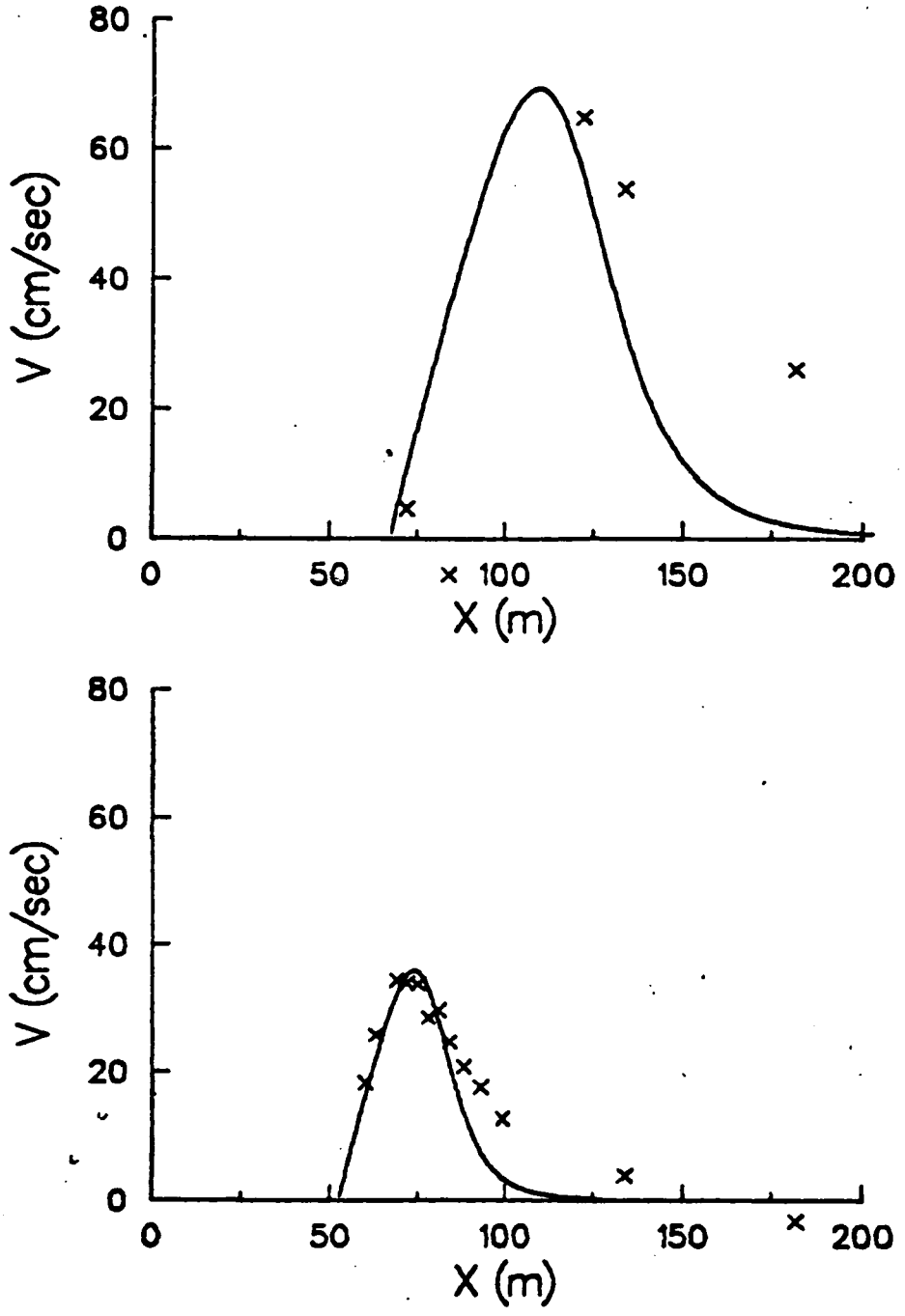

Figure (6.3). Longshore current (68-minute average) as a function of offshore distance compared with measurements indicated by x. The model is applied to data on; (a) 17 Feb., showing only a few instruments working; (b) 5 Feb., for which c_f = 0.005 was found to give the best fit.

be governed by the longshore current (Fig. 6.4). The influence of rapid depth changes is reflected in the small perturbation of the V and $\bar{q}_s$ curves at x = 65 m, which is associated with a local flatness of the beach slope, as can be seen in the "mean beach profile," Fig. 4.1. The maximum waveheight is used to define a "mean breaker line" location, x_b, for discussion purposes and normalization of the results. The analytical model is applied to a plane sloping beach. A slope of 0.037 was found as the best fit to the "mean beach" profile using Fig. 4.1. The normalized distributions resulting from the analytical model are summarized in Fig. 6.5, giving the maximum sand transport at $x/x_b \simeq 0.80$, which is similar to the results of Komar (1977a).

Comparison between the sand transport distributions using the numerical and analytical models is given in Fig. 6.6.

The sand transport peak of the numerical model, which uses the actual bathymetry, is shifted offshore compared with the analytical distribution using a planar sloping beach. It may be seen in equation (5.18) that $\bar{q}_s$ is proportional to $(\frac{1}{h})$, which means $\bar{q}_s$ increases as h decreases for the same location. The actual bottom profile (Fig. (4.1)) used in the numerical model is deeper near the breaker line compared with the plane sloping beach used in the analytical model; therefore, the calculated maximum $\bar{q}_s$ in the numerical model is shifted offshore relative to the analytical model.

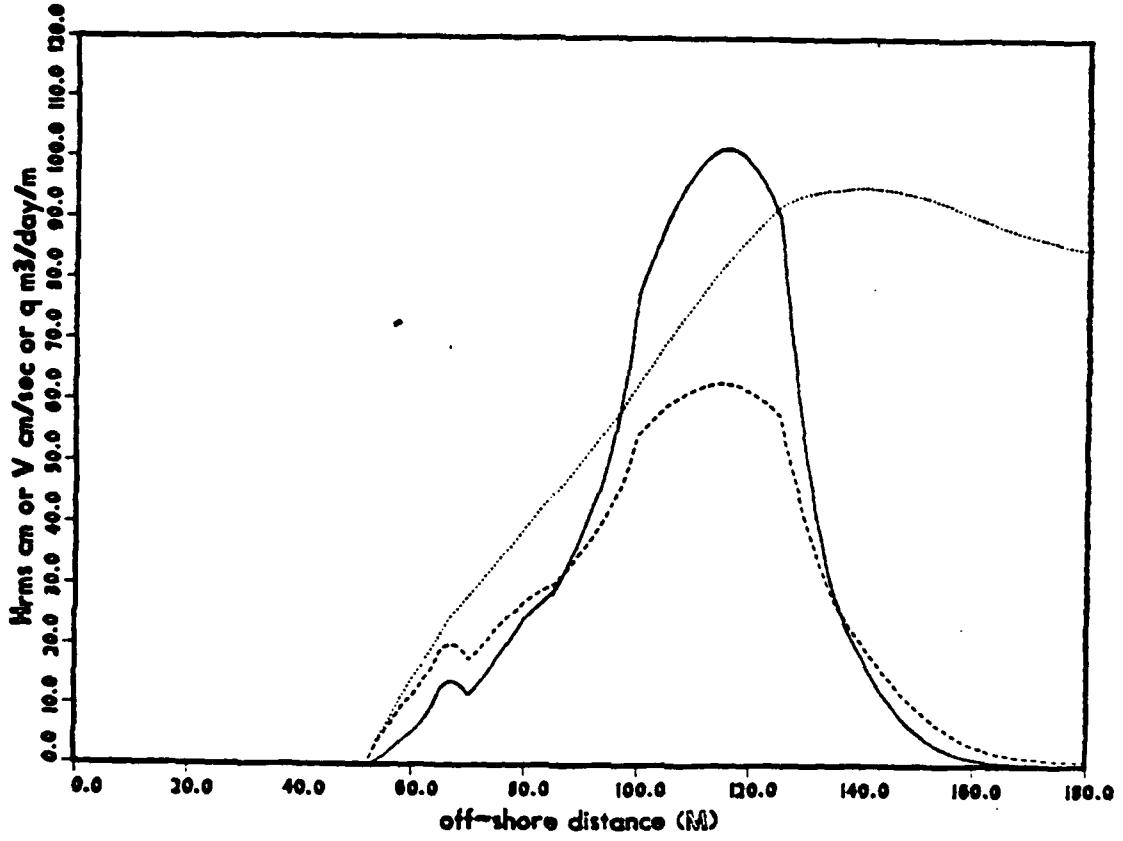

Figure (6.4). Model predictions of H_{rms} (····), V (----) and $\overline{q}_s$ (——) for actual bathymetry holding depth constant.

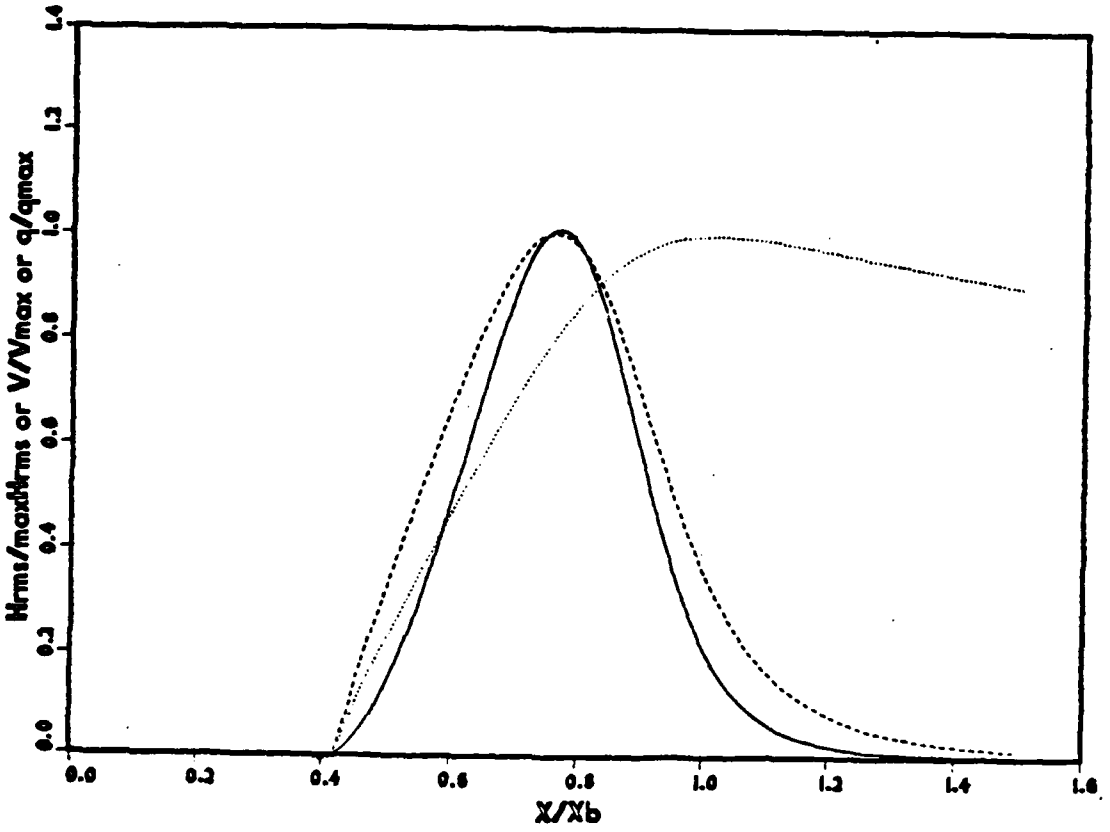

Figure (6.5). Normalized distribution for H_{rms}, V and $\bar{q}_s$ calculated by the analytical model (constant depth); H_{rms} (····), V (----) and $\bar{q}_s$ (——).

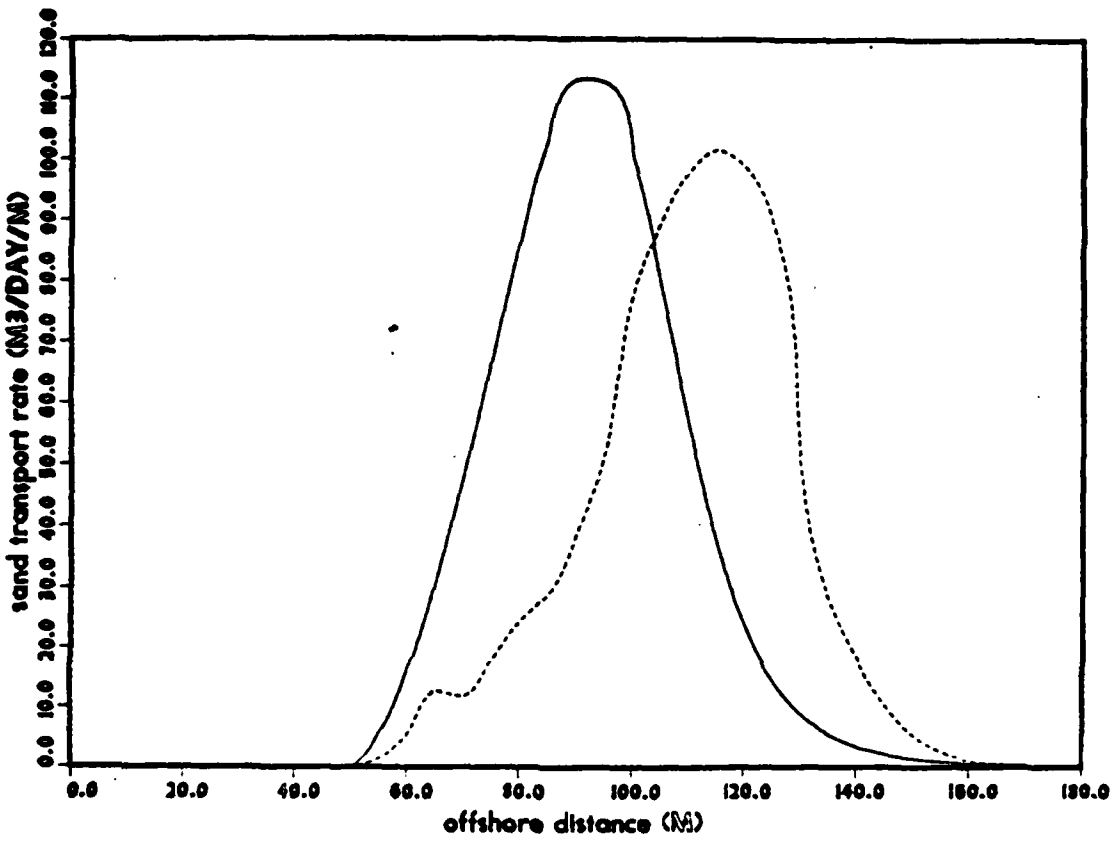

Figure (6.6). Average sand transport distribution calculated for constant depth case; for analytical model (———) and numerical model (----).

2. Model Results for Time-Varying Water Depth

The models predicting H_{rms}, V and $\bar{q}_s$ were run for the 25 hours using a one hour time step and correcting the depths for the tidal elevations at each time step. The resulting 25 sand transport distributions were averaged over the 25 hours to give a predicted mean longshore sand transport distribution between profile surveys on 17 and 18 February.

Mean sand transport distributions including tidal variation of both the analytical and numerical models are given in Fig. 6.7 which shows a good agreement with a peak shift towards offshore for the numerical model following the previous discussion. When considering the tides, the averaging causes the distribution to spread onshore to x = 30 m with less $\bar{q}_{s\,max}$ than the first case for the same coefficients. In both cases the maximum longshore sand transport occurs at almost the same location as the longshore current which indicates again that the sand transport is primarily driven by the longshore component in both models. The sediment transport distribution predicted by the numerical model is not smooth, unlike the analytical curve. This is because of the use of the actual depth profile.

C. MODEL RESULTS AND COMPARISON WITH PROTOTYPE FIELD DATA

The net longshore transport rate distribution for Santa Barbara Beach is calculated using the profile changes during

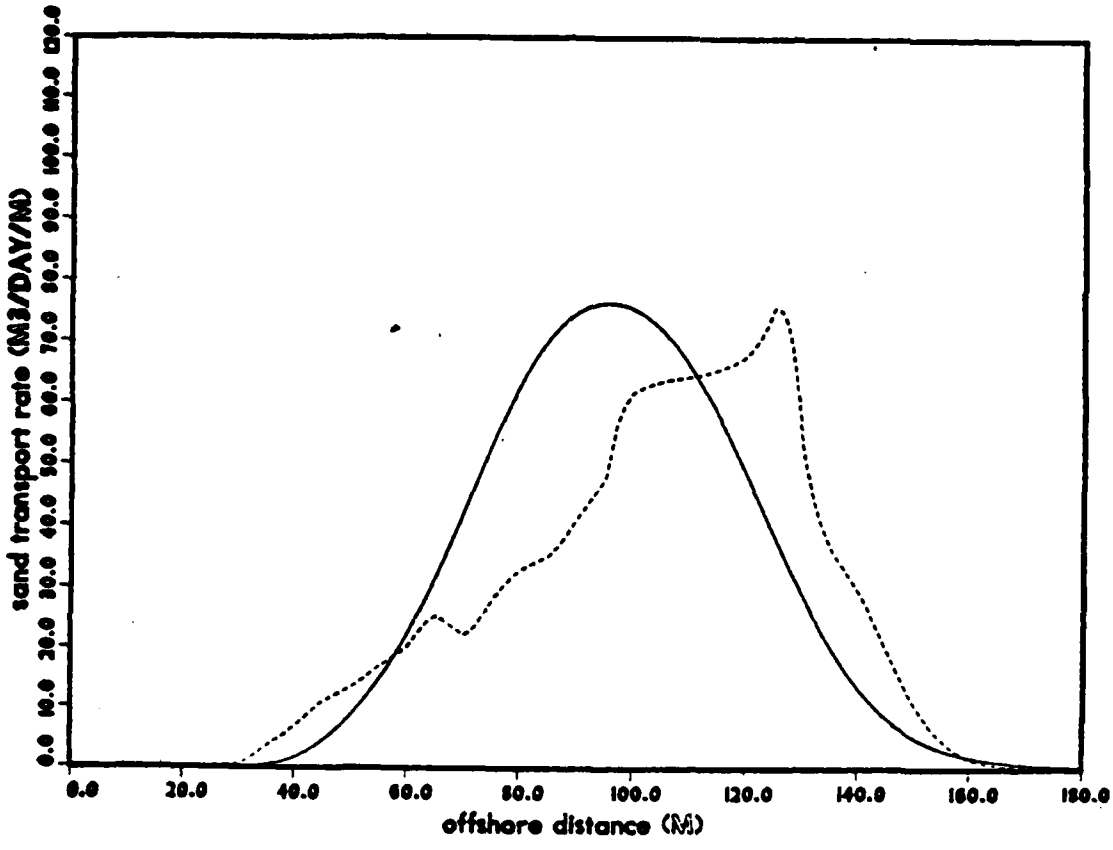

Figure (6.7). Average sand transport distribution over the daily tidal cycle calculated using variable depth; for analytical model (———) and numerical model (----).

17 and 18 February. Most of the estimated sediment transport occurs at a distance 20 m from the baseline indicating a significant beach face erosion, which is beyond the scope of the present study.

Since the volume sand transport rate calculated from the data is the net volume change rate in the beach profile, and does not represent the total longshore sand transport as the model predicts, care must be taken in the interpretation of the comparisons.

A dimensionless sand transport distribution for the field data is compared with results from the numerical model in Fig. (6.8). The measured maximum net longshore sand transport occurs on the beach face at $x \tilde{=} 20$ m. The hypothesis that the predicted longshore transport distribution is proportional to the net sediment transport distribution, calculated from the profile changes does not appear to be the case. Significant profile changes occur at the beach face which are not included in the model calculations. It is also possible that the sand eroded from the beach face was moved in the offshore direction outside 100 m and was not included in the measured profiles, which would also invalidate the original hypothesis.

D. THE EMPIRICAL COEFFICIENT B_s AND LONGSHORE SAND TRANSPORT

The empirical coefficient B_s, as described by Thornton (1973), has a magnitude of order (1) and is equal to

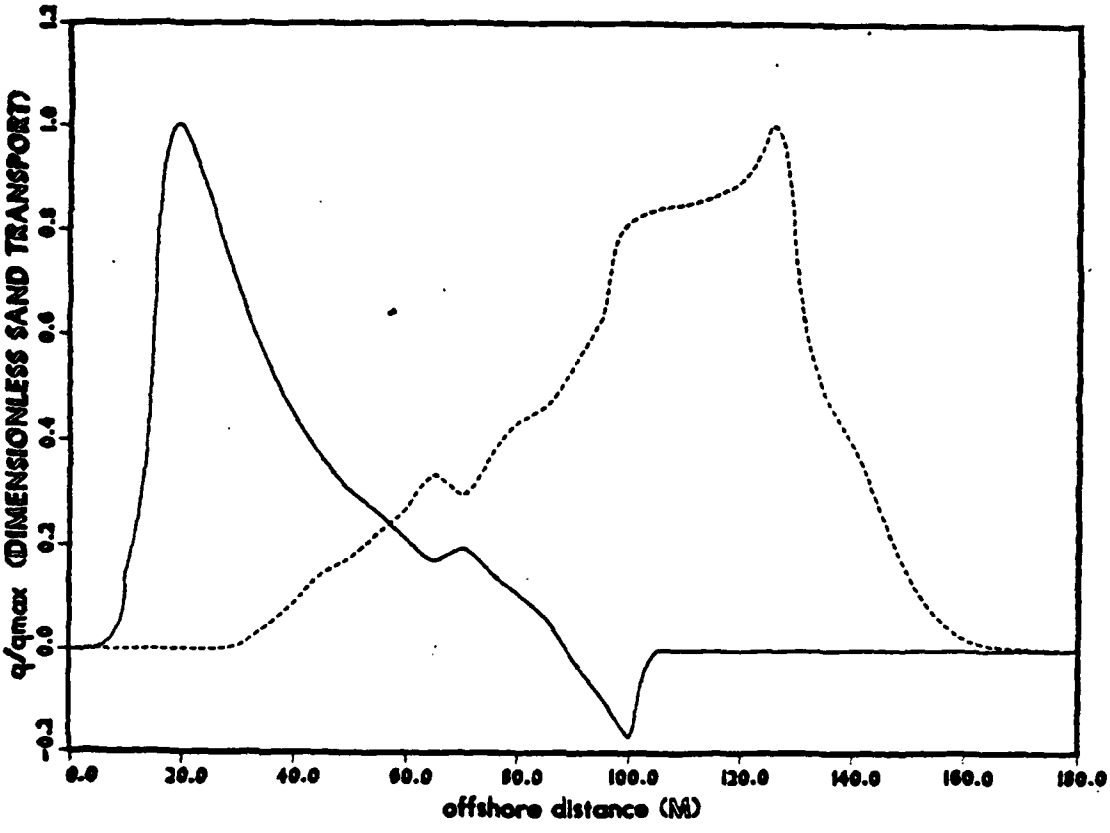

Figure (6.8). Normalized sand transport distribution inferred from profile changes vs. numerical model results with variable depth.

$$B_s = \frac{e}{b\, f_h'} \qquad (6.1)$$

where e is the transport efficiency of the available wave power and f_h' is the dynamic friction factor associated with sediment transport. The factor f_h' is equal to:

$$f_h' = \frac{\text{sediment shear stress}}{\text{normal stress at the bottom}},$$

while b is a proportionality coefficient between the ratio of sand velocities $(\frac{u}{v})_s$ and the square root of the water particle velocity ratio $(\frac{u}{v})_w^{1/2}$.

Because the data do not provide information about each individual parameter, all parameters are combined in B_s, which is determined empirically by model calibration.

The total longshore sediment transport rate (Q_ℓ) in (m^3/day) is calculated by integrating the area under the sand transport distribution

$$Q_\ell = \int_0^{x=180} \bar{q}_s \, dx$$

The calculation based on profile changes does not give the total longshore sand transport but gives the net transport which is much less in this case than the longshore transport predicted by the model. Therefore, equation (2.5) suggested by CERC (1977) is used as a reference to calibrate the longshore sand transport model.

The calculations of the longshore sand transport rate Q_ℓ require the wave condition at the breaker line H_{rmsb}, h_b and $\bar{\alpha}_b$. Field data give H_{rmsb} equal to 0.98 m, Fig. (6.2a) and h_b to be 2.96 m knowing the beach slope besides the angle $\bar{\alpha}_b$ equals six degrees from the refraction diagram, Fig. (4.4). Q_ℓ calculated using equation (2.6) gives 4600 m^3/day, which requires B_s to be 0.18.

A summary of the results if given in Table III. The difference between the two cases of depth (constant and varying) for the analytical model, was found to be insignificant. A similar result was found for the numerical model. The calculated Q_ℓ using the numerical model is less than Q_ℓ calculated from the analytical model, because the numerical model used the actual bottom profile. The numerical and the analytical models gave essentially the same maximum cross-shore transport distribution q_{max} for the same case of either constant or varying depth, Fig. (6.6) and Fig. (6.7).

Johnson (1953) estimated the longshore sand transport at Santa Barbara Beach to be 220,000 m^3/year, or about 600 m^3/day on the average. The Q_ℓ predicted by the model gives almost eight times the above estimated average daily rate. The high value of Q_ℓ predicted by the model reflects the storm conditions, which caused significant longshore transport.

TABLE III

Summary of the Results

Model	Depth Type	X_b (m)	h_b (m)	H_{rmsb} (cm)	V_b (cm/sec)	q_b (m^3/day/m)	V_{max} cm/sec	q_{max} m^3/day/m	Q_{model} m^3/day	Q_{CERC} m^3/day
Analytical	constant	120.0	2.58	94.0	-25.0	24.0	-70.0	113.0	4596.0	4600.0
	varying	135.0	2.93	91.0	-20.0	20.0	-55.0	76.0	4533.0	4600.0
Numerical	constant	140.0	2.74	95.0	-20.0	18.0	-63.0	101.0	4293.0	4600.0
	varying	145.0	3.11	94.0	-18.0	20.0	-49.0	76.0	4297.0	4600.0

Remarks:

*Distance offshore (x) is measured from the experimental baseline

This table is based on model coefficients:

$B_s = 0.184$, $B = 1.1$, $c_f = 0.005$, $\gamma = 0.44$

VII. SUMMARY AND CONCLUSIONS

The principle objective of this study is to predict the longshore sediment transport distribution. Special emphasis was placed on testing an analytical and numerical model against field data acquired from an experiment at Leadbetter Beach, Santa Barbara during the intensive storm period 17 to 18 February, 1980.

Field data show a strong longshore current coupled with significant changes in the beach profile with no evidence of on-offshore sand movement (bars or troughs) along the profiles. Therefore, it is hypothesized that the changes in the profiles are due to the variations of sand transported alongshore by the observed longshore current, and that the on-offshore sand transport is negligible. The net sand transport calculated from the profile changes is expected to have a distribution similar to the cross-shore sand transport distribution.

Initial values for the models of H_{rms_o}, $\bar{\alpha}_o$ and f_p are obtained from the field data. Model coefficients $\gamma = 0.44$, $B = 1.1$ and $c_f = 0.005$ are determined by model fitting. The developed model is capable of predicting the increase in wave height due to shoaling and the decrease after wave breaking. The model predicts the longshore current (V) and the longshore sand transport ($\bar{q}_s$) at each location. A maximum $\bar{q}_s$ is

predicted at distance $x = 0.8\ x_b$ which agrees with Komar (1977a). The experimental transport coefficient, B_s, is found to be 0.18 instead of 0.08 by Thornton (1973). The maximum longshore current, V_{max}, occurs at approximately the same location as $(\bar{q}_s)_{max}$, indicating that the sand transport distribution is primarily determined by the longshore current distribution.

The net change in the beach profiles used to infer the net sand transport distribution, shows $\bar{q}_s$ maximum at the beach face. Since the sand transport model does not consider the swash region, the net profile change distribution does not agree well with the predicted cross-shore distribution, and the original hypothesis does not appear to be valid. As a result, sand transport mechanics in the swash zone appear to be important in determining why the maximum sand transport occurs at the beach face. The swash is driven primarily by infragravity waves (long waves) due to surf beat and edge waves which have not been included in the surf zone models where only the depth-limited sea-swell frequency band of waves are considered. Therefore, further studies need to model the swash zone in order to describe the onshore water wave boundaries in a more realistic manner.

LIST OF REFERENCES

Bagnold, R.A. (1963). "Mechanics of marine sedimentation," in The Sea: Ideas and Observations, volume 3. New York, N.Y., Interscience Publishers, 1963, pp. 507-528.

Bailard, J.A., and D.L. Inman (1981). "An energetics bedload transport model for a plane sloping beach; Local transport," Journal of Geophysical Research, Vol. 86, No. 3, 1981, pp. 2035-2043.

Bailard, J.A. (1982). "An energetics total load sediment transport model for a plane sloping beach," Technical note, Naval Civil Engineering Laboratory, Port Hueneme, CA 93043, TN No: N-1626.

Bowen, A.J. (1981). "Simple models of nearshore sedimentation; beach profiles and longshore bais," in Proceedings of the Conference on Coastline of Canada, Halifax, 1978, Geological Survey of Canada.

CERC (1977). "Shore Protection Manual," U.S. Army Corps of Engineers, Coastal Engineering Research Center, Vol. I.

Gable, C.G. (1981). Report on data from the nearshore sediment transport study experiment at Leadbetter Beach, Santa Barbara, CA, January-February, 1980, Institute of Marine Research, IMR Ref. No. 85-5. La Jolla, Calif.

Inman, D.L., and R.A. Bagnold (1963). "Littoral Processes," in The Sea: Ideas and Observations, volume 3. New York, N.Y., Interscience Publishers, 1963, pp. 529-533.

Komar, P.D., and D.L. Inman (1970). "Longshore sand transport on beaches," Journal of Geophysical Research, vol. 75, no. 30, 1970, pp. 5914-5927.

Komar, P.D. (1971). "The mechanics of sand transport on beaches," Journal of Geophysical Research, vol. 76, no. 3, 1971, pp. 713-721.

Komar, P.D. (1977). "Beach sand transport: Distribution and total drift," Proceedings of ASCE Journal of Waterways, Harbors and Coastal Engineering, WW4, May 1977, pp. 225-239.

Komar, P.D. (1976). Beach Processes and Sedimentation, Prentice-Hall, Inc., Englewood Cliffs, N.J., 1976.

Komar, P.D. (1983). "Nearshore currents and sand transport on beaches," Coastal and Shelf Dynamical Processes, edited by Brayan Johns, Elsevier Press, in press.

Kraus, N.C., R.S. Farinato, and K. Horikawa (1981). "Field experiments on longshore sand transport in the surf zone," Coastal Engineering in Japan, vol. 24, 1981.

Liu, Ph. L-F and R. Dalrymple (1978). "Bottom frictional stresses and longshore currents due to waves with large angles of incidence," Journal of Marine Research, volume 36, no. 2, 1978, pp. 357-375.

Longuet-Higgins, M.S. (1953). "Mass transport in water wavys," Philosophical Transactions of the Royal Society, London, Series A, vol. 245, 1953, pp. 535-581.

Longuet-Higgins, M.S. (1970). "Longshore currents generated by obliquely incident sea waves, 1", J. Geophys. Res., 75, pp. 6778-6789.

Longuet-Higgins, M.S. (1972). "Recent progress in the study of longshore currents," in Waves on Beaches and Resulting Sediment Transport, R.E. Meyer, Editor. New York, N.Y., Academic Press, 1972, p. 462.

Madsen, O.S., and W.D. Grant (1976). "Sediment transport in the coastal environment," Massachusetts Institute of Technology, Department of Civil Engineering, Ralph M. Parsons Laboratory, Report No. 241, 1976, p. 105.

Mizuguchi, M., and M. Mori (1981). "Modeling of two-dimensional beach transformation due to waves," Coastal Engineering in Japan, vol. 24, 1981, pp. 155-170.

Sawaragi, T. and I. Deguchi, (1978). "Distribution of sand transport rate across the surf zone," Proceedings 16th Coastal Engineering Conference, ASCE, Pp. 1596-1613.

Seymour, R.J., and D.B. King (1982). "Field comparisons of cross-shore transport models," Journal of the Waterway Port Coastal and Ocean Division, May 1982, Pp. 163-179.

Thornton, E.B. (1973). "Distribution of sediment transport across the surf zone," in Proceedings of the 13th Conference on Coastal Engineering. American Society of Civil Engineers, 1973, Pp. 1049-1068.

Thornton, E.B., and R.T. Guza (1982). "Transformation of wave height distribution," Journal of Geophysical Research.

Thornton, E.B., and R.T. Guza (1983). "Longshore currents due to random waves," submitted to the Journal of Geophysical Research.

Vitale, P. (1981). "Movable-bed laboratory experiments comparing radiation stress and energy flux factor as predictors of longshore transport rate," U.S. Army, Corps of Engineers Coastal Engineering Research Center, Fort Belvoir, VA 22060, MR No. 81-4.

Wang, Y-H., and T.H. Chang, (1979). "Littoral drift along bayshore of a barrier island," Proceedings, 16th Conf. on Coastal Engineering, Pp. 1614-1625.

INITIAL DISTRIBUTION LIST

		No. Copies
1.	Defense Technical Information Center Cameron Station Alexandria, VA 22314	2
2.	Library, Code 0142 Naval Postgraduate School Monterey, CA 93940	2
3.	Chairman, Code 68Mr Department of Oceanography Naval Postgraduate School Monterey, CA 93940	1
4.	Chairman, Code 63Rd Department of Meteorology Naval Postgraduate School Monterey, CA 93940	1
5.	Prof. E.B. Thornton, Code 68 Department of Oceanography Naval Postgraduate School Monterey, CA 93940	1
6.	Saad Abdelrahman SMC 2251 Naval Postgraduate School Monterey, CA 93940	1
7.	Director Naval Oceanography Division Naval Observatory 34th and Massachusetts Avenue NW Washington, D.C. 20390	1
8.	Commander Naval Oceanography Command NSTL Station Bay St. Louis, MS 39522	1
9.	Commanding Officer Naval Oceanographic Office NSTL Station Bay St. Louis, MS 39522	1
10.	Commanding Officer Fleet Numerical Oceanography Center Monterey, CA 93940	1

11. Commanding Officer — 1
Naval Ocean Research and
Development Activity
NSTL Station
Bay St. Louis, MS 39522

12. Commanding Officer — 1
Naval Environment Prediction
Research Facility
Monterey, CA 93940

13. Chairman, Oceanography Department — 1
U.S. Naval Academy
Annapolis, MD 21402

14. Chief of Naval Research — 1
800 N. Quincy Street
Arlington, VA 22217

15. Office of Naval Research (Code 480) — 1
Naval Ocean Research and
Development Activity
NSTL Station
Bay St. Louis, MS 39522

16. Scientific Liaison Office — 1
Office of Naval Research
Scripps Institution of Oceanography
La Jolla, CA 92037

17. Library — 1
Scripps Institution of Oceanography
P.O. Box 2367
La Jolla, CA 92037

18. Library — 1
Department of Oceanography
University of Washington
Seattle, WA 98105

19. Library — 1
CICESE
P.O. Box 4803
San Ysidro, CA 92073

20. Library — 1
School of Oceanography
Oregon State University
Corvallis, OR 97331

21. Commander — 1
Oceanographic Systems Pacific
Box 1390
Pearl Harbor, HI 96860